Acta Crystallogr. A **32**
A B A
Ferroelectrics **11**
A *Electroceramics: Materials, Properties, Applications* ( )
J. Mater. Res. **18**
B *Appl. Phys.* A **65**
B *Phase Transit.* **79**
A *Phase Transit.* **79**
Mineralog. Mag. **61**

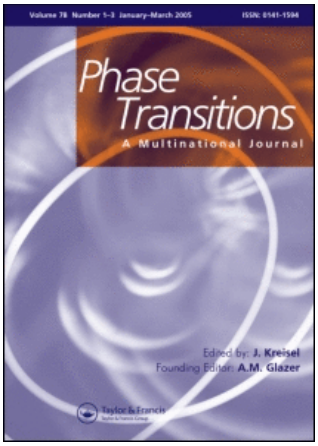

Phase Transitions
A Multinational Journal
Publication details, including instructions for authors and subscription information:
http://www.informaworld.com/smpp/title~content=t713647403

Effects of strontium on the characteristics of $Pb(Zr_{1/2}Ti_{1/2})O_3$--$Pb(Zn_{1/3}Nb_{2/3})O_3$ ceramics

Online Publication Date: 01 August 2007
To cite this Article: Vittayakorn, N. , (2007) 'Effects of strontium on the characteristics of $Pb(Zr_{1/2}Ti_{1/2})O_3$--$Pb(Zn_{1/3}Nb_{2/3})O_3$ ceramics', Phase Transitions, 80:8, 813 - 821
To link to this article: DOI: 10.1080/01411590701288038
URL: http://dx.doi.org/10.1080/01411590701288038

Phase Transitions,
Vol. 80, No. 8, August 2007, 813–821

Effects of strontium on the characteristics of $Pb(Zr_{1/2}Ti_{1/2})O_3$–$Pb(Zn_{1/3}Nb_{2/3})O_3$ ceramics

N. VITTAYAKORN*

Materials Science Research Unit, Department of Chemistry, Faculty of Science, King Mongkut's Institute of Technology Ladkrabang, Bangkok 10520, Thailand

(*Received 18 December 2006; in final form 19 February 2007*)

The dielectric and piezoelectric properties of pyrochlore-free lead zirconate titanate-lead zinc niobate ceramics were investigated systematically as a function of Sr doping. The powders of $Pb_{(1-x)}Sr_x[0.7(Zr_{1/2}Ti_{1/2})–0.3(Zn_{1/3}Nb_{2/3})]O_3$, where $x = 0$–0.06 were prepared using the columbite-(wolframite) precursor method. The ceramic materials were characterized using X-ray diffraction, dielectric spectra, hysteresis and electromechanical measurements. The phase-pure perovskite phase of Sr-doped PZN–PZT ceramics was obtained over a wide compositional range. The results showed that the optimized electrical properties were also achieved at composition $x = 0.0$, which were $K_P = 0.69$, $d_{33} = 670\,pC\,N^{-1}$, $P_r = 31.9\,\mu C\,cm^{-2}$ and $\varepsilon_{rmax} = 18600$. Maximum dielectric constant values of the systems decreased rapidly with increasing Sr concentration. Moreover, with increasing Sr concentration dielectric constant *versus* temperature curves become gradually broader. The diffuseness parameter increased significantly with Sr doping. Furthermore, Sr doping has been shown to produce a linear reduction in the transition temperature (T_m) $= 294.1–12.7x°C$ with concentration (x). Sr shifts the transition temperature of this system at a rate of $12.7°C\,mol^{-1}\%$.

Keywords: $Pb(Zr_{1/2}Ti_{1/2})O_3$; $Pb(Zn_{1/3}Nb_{2/3})O_3$ dielectric properties; Perovskite structure

1. Introduction

Piezoelectric materials are widely used for various devices, including multilayer capacitors, sensors, and actuators. By the 1950s, the ferroelectric solid solution $Pb(Zr_{1-x}Ti_x)O_3$ (PZT) was found to host exceptionally high dielectric and piezoelectric properties for compositions close to the morphotropic phase boundary (MPB). This MPB is located around $PbZrO_3 : PbTiO_3 \sim 0.52 : 0.48$ and separates a Ti-rich tetragonal phase from a Zr-rich rhombohedral phase [1, 2]. Recent results have discovered the existence of a low-symmetry (monoclinic) phase within the MPB region, a nearly vertical line between the rhombohedral and tetragonal phases [3]. And Noheda *et al*. [4, 5] and [6] have suggested that the enhanced dielectric

*Email: naratipcmu@yahoo.com

Phase Transitions
ISSN 0141-1594 print/ISSN 1029-0338 online © 2007 Taylor & Francis
http://www.tandf.co.uk/journals
DOI: 10.1080/01411590701288038

and piezoelectric properties around the MPB are due to the formation of an intermediate monoclinic phase.

Most commercial PZT ceramics are thus designed in the vicinity of the MPB with various dopings in order to achieve optimum properties. Ions of alkaline–earth metals, e.g., Ca^{2+}, Sr^{2+} and Ba^{2+} which have ionic radii of 1.06 Å, 1.27 Å and 1.43 Å, respectively, are frequently used to substitute for Pb^{2+} [2, 7]. Recently, Zheng *et al*. [8] have reported that Sr-modified PZT ceramics generally have higher dielectric and piezoelectric properties than pure PZT. Sr substitutions on the A-site in PZT tended to shift the MPB composition toward the tetragonal phase.

Lead zinc niobate, $Pb(Zn_{1/3}Nb_{2/3})O_3$, (PZN) has a disordered complex perovskite structure in which Zn^{2+} and Nb^{5+} cations are distributed randomly with the short range ordering on the B-site [9]. PZN is a well known relaxor ferroelectric that has been noted for its high permittivity and extremely high piezoelectric coefficients [10]. Relaxor single crystal actuators can produce strain levels in excess of 1% and exhibit five times the strain energy density of conventional piezo-ceramics [11]. These materials are used for compact chip capacitors, actuators, hydrophones, sonar transducers, receivers and micro-positioning devices [12–14]. Although single crystals of PZN can routinely be grown by the flux method [11], it is known that perovskite PZN ceramics cannot be synthesized by the conventional mixed-oxide method without doping [15]. It is well known that replacement of the A-site ion (Pb) by an ion with a large radius such as Ba or Sr is also considered to be a good approach to stabilize the perovskite phase [15]. Such an approach is also known to improve the mechanical strength, increase the electrical resistivity, and of course reduce the total amount of Pb weight% in the composition. Recently our previous work [16, 17] observed large coupling coefficients and large piezoelectric constants in PZN–PZT ceramics. This study is concerned with the effect of Sr substituted PZT modified with the relaxor ferroelectric PZN. Based on our previous [16] results for the PZN–PZT system, PZT containing 30 mol% of PZN was selected as the starting composition which is close to the rhombohedral MPB in this system.

2. Materials and methods

The general formula of the materials studied was $Pb_{(1-x)}Sr_x[0.7(Zr_{1/2}Ti_{1/2})\ 0.3(Zn_{1/3}Nb_{2/3})]O_3$, where $x = 0$–0.06. The samples were prepared by the two-stage method to acquire a pure phase of perovskite. Reagent-grade oxide powders, PbO, ZrO_2, TiO_2, ZnO, Nb_2O_5, and $SrCO_3$, were used as the starting materials. In the first stage, a powder of columbite precursor, $ZnNb_2O_6$, was prepared by calcination of ZnO with Nb_2O_5 at 1100°C for 4 h. And the wolframite precursor, $ZrTiO_4$, were synthesized by calcination of ZrO_2 with TiO_2 at 1400°C for 4 hours In the second stage, the above precursor with PbO, $ZrTiO_4$, $ZnNb_2O_6$, and $SrCO_3$ was weighed and mixed through use of a polyethylene jar and ZrO_2 milling media. The mixture was then calcined at 900°C for 4 h in air, remilled, pressed into disks ~10.0 mm in diameter at around 80 MPa, and then sintered at 1200°C for 2 h in a sealed alumina crucible with a $PbZrO_3$ powder atmosphere. The as-sintered disks were lapped and electroded with a silver paste. The specimens for piezoelectric properties measurements were poled in a silicone oil bath with a DC field of 3 kV mm^{-1} for

45 min at 120°C and was cooled down to room temperature under a DC field. The specimens were aged for 24 h before testing.

The crystal structure of solid solutions was analyzed using X-ray diffractometry XRD (PW1729, Philips, Netherlands) with a 2θ range from 10° to 60°. A step scan with a step size of 0.02° was used with a counting time of 1 s/step. The bulk density was measured using the Archimedes method. The piezoelectric constant (d_{33}) was measured using a quasi-static piezoelectric d_{33} meter (Model 8000 d_{33} Tester). The planar coupling coefficient (k_p) was determined by the resonance and anti-resonance technique using an impedance analyzer (Model HP4194A, Hewlett-Packard, CA). The transition temperature (T_m) and dielectric constant (K) were measured on heating at $3°C\,min^{-1}$ using an LCR meter (HP4274A, Hewlett-Packard, Palo Alto, CA) over the range of 100 Hz to 500 kHz and temperatures of 25 to 450°C. In addition, the polarization (P) was measured as a function of electric field (E), using a ferroelectric tester system (Radiant Technologies, Inc., PT66A).

3. Results and discussion

Figure 1 shows the XRD diffraction patterns of $Pb_{(1-x)}Sr_x[0.7(Zr_{1/2}Ti_{1/2})\ 0.3(Zn_{1/3}Nb_{2/3})]O_3$, where $x = 0$–0.06 specimens, each exhibiting a phase-pure perovskite phase within the detection limit of the equipment. It is apparent that no undesirable pyrochlore phase such as $Pb_2Nb_2O_7$ or $Pb_{1.83}(Zn_{0.29}Nb_{1.71})O_{6.39}$ has been formed because no diffraction peaks are observed in the 2θ range of 28–30°,

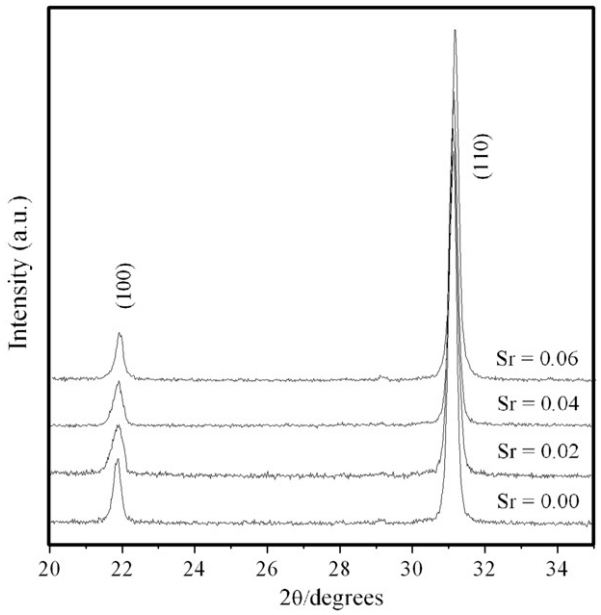

Figure 1. Room Temperature XRD patterns of PZT–PZN (ZT : ZN = 70 : 30) ceramics as function of Sr-doping level.

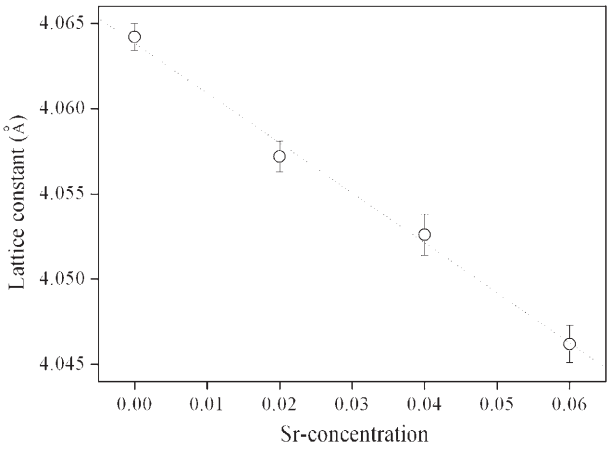

Figure 2. Lattice parameter (Å) of perovskite structure as a function of Sr concentration.

in which their strongest diffraction peaks are (JCPDS 25-0444, 34-0374). The XRD data can be identified as a single-phase material with a perovskite structure, having rhombohedral symmetry. With the peaks properly indexed, lattice parameter was determined using UnitCell, a linear least squares refinement program. The calculated lattice parameters of the perovskite structures are presented in figure 2. An increase in the mole faction of Sr^{2+} did not show any evidence of a change in symmetry. Also, the lattice constant linearly decreases with the replacement of Pb^{2+} by Sr^{2+} according to the Vegard rule.

It indicates that, together with the XRD patterns in figure 1, complete series of perovskite solid solutions are formed. In general, the lattice parameters of the perovskite structure also decreased gradually as x increased, undoubtedly because of the introduction of the smaller strontium ion ($r = 1.27$ Å) into the lead site ($r = 1.49$ Å), resulting in decreasing of the unit cell. Bulk density of piezo-ceramics is an important factor influencing the properties of ceramics. Commonly, the dielectric and piezoelectric properties of ferroelectric materials depend strongly on chemical compositions as well as the density of the specimens. The densities of the as-sintered specimens containing different amounts of strontium were measured, and the results are shown in figure 3. The densification behaviour of the specimen was greatly influenced by the strontium content. The density decreased almost linearly with increasing strontium concentration for both of the samples.

Dielectric constant or relative permittivity *versus* temperature measurements of as-sintered samples are summarized in figure 4. All of the samples displayed relaxor ferroelectric behaviour, characterized by broad frequency and temperature dependent phase [18]. As the Sr^{2+} content increased, a clear shift of the transition temperature to lower temperatures was observed. In addition, the dielectric maximum decreased as the x value increased. Furthermore the dielectric peak became broader as the Sr content increased. The broad dielectric spectra of the relaxor ferroelectric composition more appropriately follow the quadratic law [19]. This arises from the fact that the total number of relaxors contributing to the permittivity response in the vicinity of the permittivity peak is temperature-dependent, and the temperature distribution of this number is given

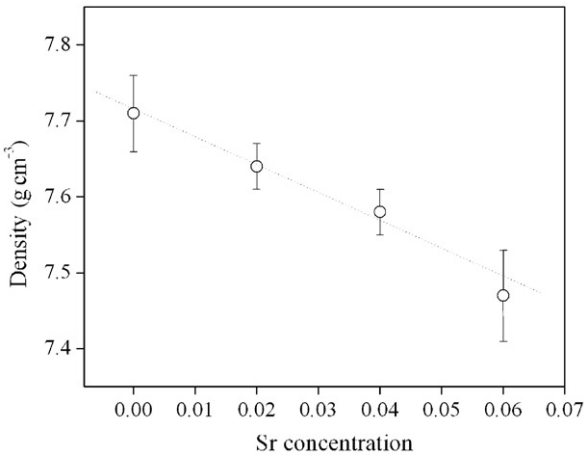

Figure 3. The density of the perovskite PZT–PZN ceramics as a function of strontium.

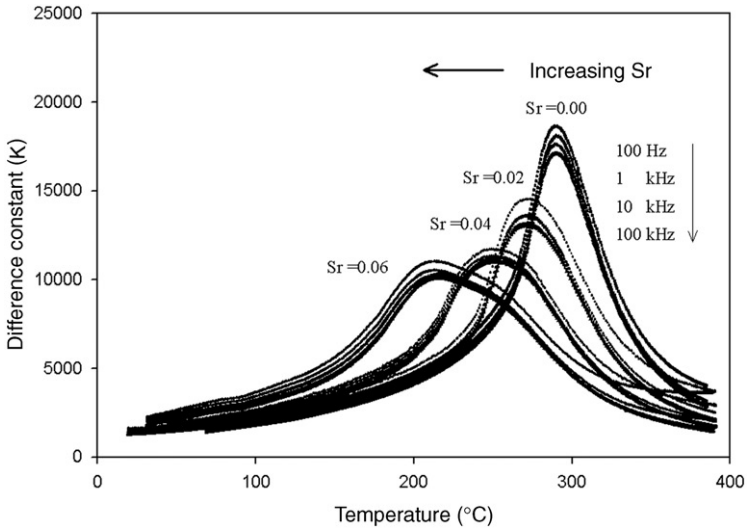

Figure 4. Dielectric properties as a function of temperature on heating at frequency of 100 Hz–100 kHz varies Sr concentration of the as-sintered sample.

by a Gaussian function about a mean value T_o with a standard deviation σ. The diffusiveness parameter (δ) of the transition was calculated from the expression [20]:

$$\frac{K_m}{K(f,T)} = \exp\left(\frac{(T - T_m(f))^2}{2\delta^2}\right) \tag{1}$$

where K_m is maximum value of the dielectric constant at $T = T_m(f)$ and $K(f, T)$ is the intrinsic dielectric constant of sample. If ln (K_m/K_g) is plotted *versus* $(T - T_m)^2$, the slope of the fitted curve, $1/(2\delta^2)$, will give the value of the diffuseness parameter. As clarified by Pilgrim *et al.* [20] the estimate of δ is valid for the range of $K_m/K_{(f,T)} < 1.5$. Table 1 gives in more detail the dielectric and ferroelectric

Table 1. Dielectric and ferroelectric properties of Sr-doped PZT–PZN ceramics.

	As-sintered				
Sr Mol	$\varepsilon_{r\,max}$	δ	P_r ($\mu C\,cm^{-2}$)	E_c ($kV\,cm^{-1}$)	R_{sq}
0.00	18600	29.0	31.9	10.6	1.48
0.02	14500	38.8	24.0	10.8	1.41
0.04	11600	48.2	20.2	11.7	1.38
0.06	11000	71.8	18.1	12.7	1.33

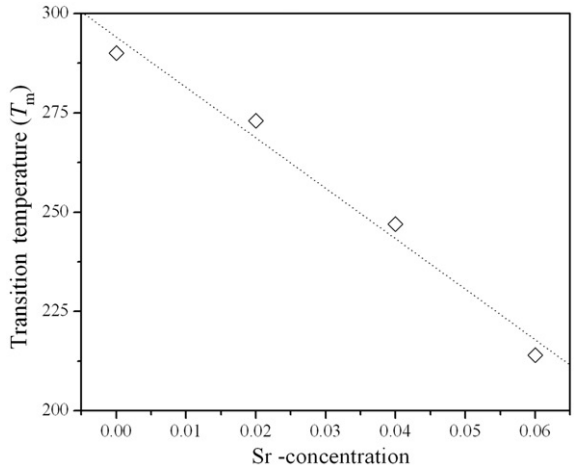

Figure 5. Transition temperature (T_{max}) of Sr doped PZT–PZN ceramic as a function of doping level.

properties of the Sr dope PZN–PZT ceramics. The diffuseness parameter increased significantly with Sr doping. It is important to note that at the composition $x = 0.06$, two peaks were revealed at temperatures ~214°C and ~250°C in the ceramics at 1 kHz. However, this behaviour was not observed at a low concentration of strontium. These two peaks are interpreted to be due to the phase transitions, or in other words associated with the possibility of the decrease of the chemical homogenization. Other authors have reported a similar behaviour [21, 22].

The transition temperature at 1 kHz *versus* the Sr content is also plotted in figure 5. As expected, S_r doping has been shown to produce a linear reduction in the transition temperature (T_m) = 294.1−12.7x°C with concentration (x). Sr shifts the transition temperature of this system at a rate of $12.7°C\,mol^{-1}\%$, which agrees quantitatively with the previous studies [22, 23]. Figure 6 display the hysteresis curves of doped PZT–PZN samples. As one can expect the polarization decreased with increasing Sr dopant concentration [24, 25]. Haertling and Zimmer [26] derived an empirical relationship between remanent polarization, saturation polarization and polarization at fields above the coercive field. This permits the quantification of changes in the hysteresis behaviour for each sample through the following equation:

$$R_{sq} = \frac{P_r}{P_s} + \frac{P_{1.1E_c}}{P_r} \tag{2}$$

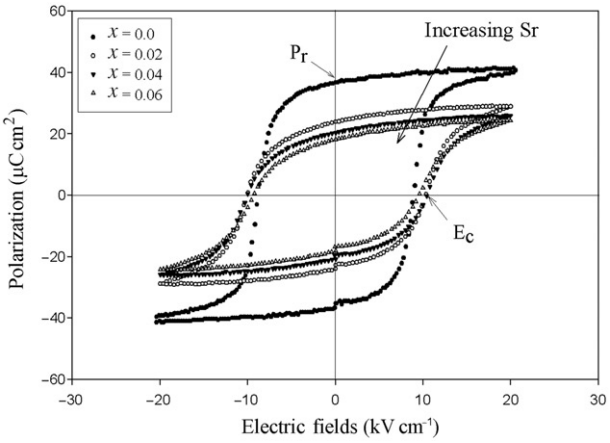

Figure 6. Dependence of the polarization *versus* electric field (*P–E*) loop on the Sr dopant.

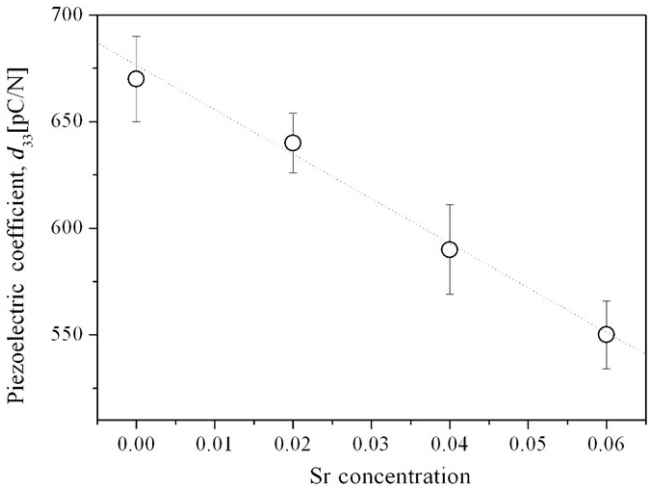

Figure 7. Piezoelectric constant (d_{33}) of PZT–PZN specimens with Sr doping concentration.

where, R_{sq} is the squareness of hysteresis loop, P_r is remanent polarization, P_s is saturation polarization, $P_{1.1Ec}$ is the polarization at an electric field equal to 1.1 times the coercive field (E_C). For an ideal hysteresis loop, the squareness parameter is equal to two. Normal square ferroelectric *P–E* loops were observed in undoped samples. The hysteresis curves also become more slanted with increasing Sr content. The remanent polarization decreased from 31.9 to 20.2 $\mu C\,cm^{-2}$ for the sample doped with 0.04 mol Sr. However, the coercive field increased from 10.6 to 12.7 $kV\,cm^{-1}$ after doping with 0.06 mol Sr. Figures 7 and 8 show the changes in the piezoelectric constant (d_{33}) and the electromechanical coupling factor (k_p) as a function of the amount of Sr addition, respectively. As can be seen, both k_p and d_{33} show a similar variation with increasing Sr content. The piezoelectric constant (d_{33}) and the electromechanical coupling factor (k_p) decreases with increasing Sr content.

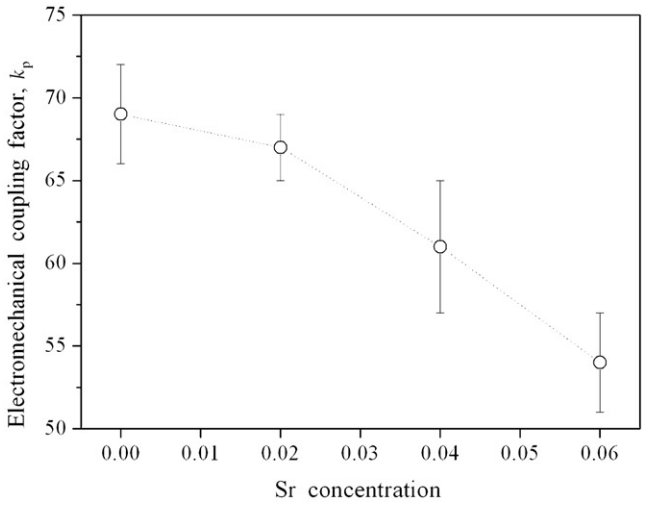

Figure 8. Electromechanical coupling factor (k_p) of PZT–PZN specimens with Sr doping concentration.

4. Conclusions

The dielectric and ferroelectric properties of Sr-modified PZT–PZN ceramics formed via the columbite process were investigated. With an increase in the Sr dopant concentration, the transition temperature and the maximum dielectric constant decreased. In addition, Sr doping caused the ferroelectric phase transition to become more diffuse.

Acknowledgements

This work was supported by The Thailand Research Fund (TRF), Commission on Higher Education (CHE) and King Mongkut's Institute of Technology Ladkrabang (KMITL). The author would like to thank Prof. Dr. Gobwuit Rujijanagul and Prof. Dr. David P. Cann for their help in many facilities.

Reference

[1] M.E. Lines and A.M. Glass, *Principles and Applications of Ferroelectrics and Related Materials* (Clarendon Press, Oxford, 1977).
[2] B. Jaffe and W.R. Cook, *Piezoelectric Ceramic* (R.A.N. Publishers, London, 1971).
[3] B. Noheda, D.E. Cox, G. Shirane, *et al.*, Appl. Phys. Lett. **74** 2059 (1999).
[4] B. Noheda and D.E. Cox, Phase Trans. **79** 5 (2006).
[5] B. Noheda, Curr. Opin. Solid State Mater. Sci. **6** 27 (2002).
[6] B. Noheda, J.A. Gonzalo, L.E. Cross, *et al.*, Phys. Rev. B **61** 8687 (2000).
[7] Y. Xu, *Ferroelectric Materials and Their Application* (Elsevier Science, Amsterdam, 1991).
[8] H. Zheng, I.M. Reaney, W.E. Lee, *et al.*, J. Eur. Ceram. Soc. **21** 1371 (2001).
[9] C.A. Randall, A.S. Bhalla, T.R. Shrout, *et al.*, Ferroelectrics **11** 103 (1990).
[10] J. Kuwata, K. Uchino and S. Nomura, Ferroelectrics **37** 579 (1981).
[11] J. Kuwata, K. Uchino and S. Nomura, Jpn. J. Appl. Phys. **21** 1298 (1982).

[12] K. Uchino, *Ferroelectric Devices* (Marcel Dekker Inc., New York, 2000).
[13] K. Uchino, *Piezoelectric Actuators and Ultrasonic Motors* (Kluwer Academic Publishers, Boston, MA, 1996).
[14] A.J. Moulson and J.M. Herbert, *Electroceramics: Materials, Properties, Applications* (Chapman and Hall, New York, 1990).
[15] T.R. Shrout and A. Halliyal, Am. Ceram. Soc. Bull. **66** 704 (1987).
[16] N. Vittayakorn, G. Rujijanagul, T. Tunkasiri, *et al*., Mat. Sci. Eng. B **108** 258 (2004).
[17] N. Vittayakorn, C. Puchmark, G. Rujijanagul, *et al*., Curr. Appl. Phys. **6** 303 (2006).
[18] L.E. Cross, Ferroelectrics **76** 241 (1987).
[19] V.V. Kirillov and V.A. Isupov, J. Mater. Res. **5** 3 (1973).
[20] S.M. Pilgrim, A.E. Sutherland and S.R. Winzer, J. Am. Ceram. Soc. **73** 3122 (1990).
[21] W. Chaisan, R. Yimnirun, S. Ananta, *et al*., Mat. Sci. Eng. B **132** 300 (2006).
[22] J. Belsick, Y. Yamashita and M. Harata, paper presented at IEEE 7th International Symposium on Applications of Ferroelectrics, Urbana-Champaign, IL, 1990, pp. 44–47.
[23] J.R. Belsick, A. Halliyal, U. Kumar, *et al*., Am. Ceram. Soc. Bull. **66** 664 (1987).
[24] G.A. Samara, J. Phys.: Condens. Matter **15** 367 (2003).
[25] G.A. Samara and E.L. Venturini, Phase Transitions **79** 21 (2006).
[26] G.H. Haertling and W.J. Zimmer, Am. Ceram. Soc. Bull. **45** 1084 (1966).

Applied Physics A
Materials Science & Processing

N. VITTAYAKORN ✉
D.P. CANN

Preparation and ferroelectric properties of pyrochlore-free $Pb(Ni_{1/3}Nb_{2/3})O_3$-based solid solutions

B

A

Received: 31 July 2006/Accepted: 3 November 2006
Published online: 14 December 2006 • © Springer-Verlag 2006

ABSTRACT

. (/ /) −(. −*x*)− (/ /)
x (/ /) *x* = . ( )

°
( ) /
(° /)

x

x = . . μ /
. μ /

PACS B

1 Introduction

(B + = +, +, + B + = +, +)
(B + B + /)

B

(B)

/ /
( )
( )
A

((/ /)
) (−*x* *x*) ( )

(ε) B

/

°

k = .
. . .

A

. (. −*x*) *x*
x = .

✉

2 Experimental procedure

– °

° / *P*
P E

– °

(. A °
A) (A ( )
A)

°

°

( )

. (. – *x*) *x* *x* =

3 Results and discussion

. / 3.1 *Perovskite-phase development*

. (. – *x*)
x *x* = .

°

° / A ( )
/ (° /)

° ° / ° A

.

( )
(
) K_α
. ° a = .
B T ≈ – °
(A)

(/ /)

(*x*) *T*

°

A

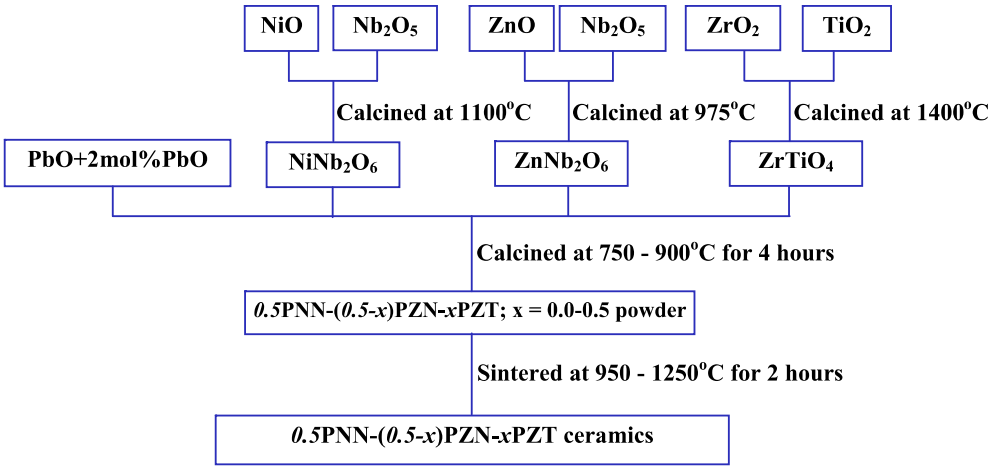

FIGURE 1 /

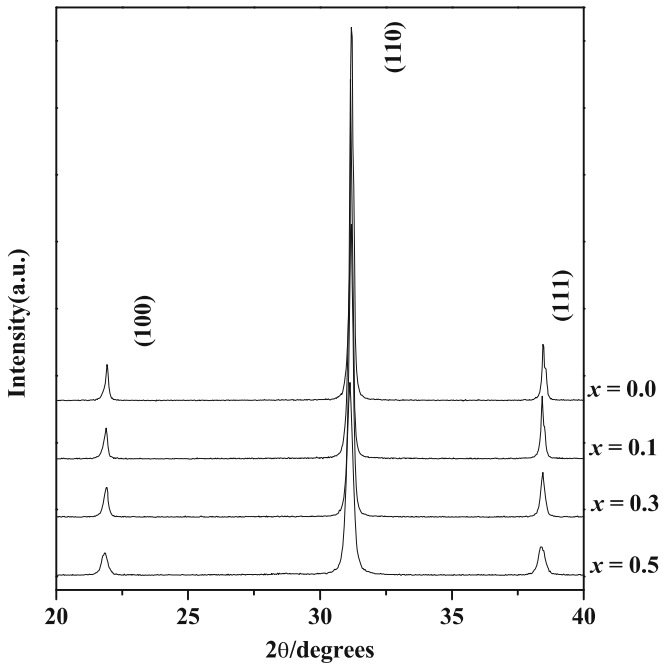

FIGURE 2 . (. −*x*) *x*

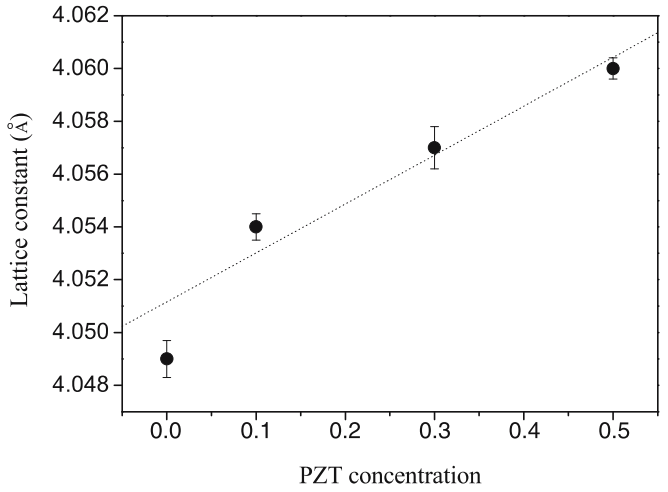

FIGURE 3 (. − *x*) *x*

x

(/ /) (*r* = .) B (/ /) (*r* = .)

3.2 *Ferroelectric and dielectric properties*

x = . *x* = *x* = .

P E

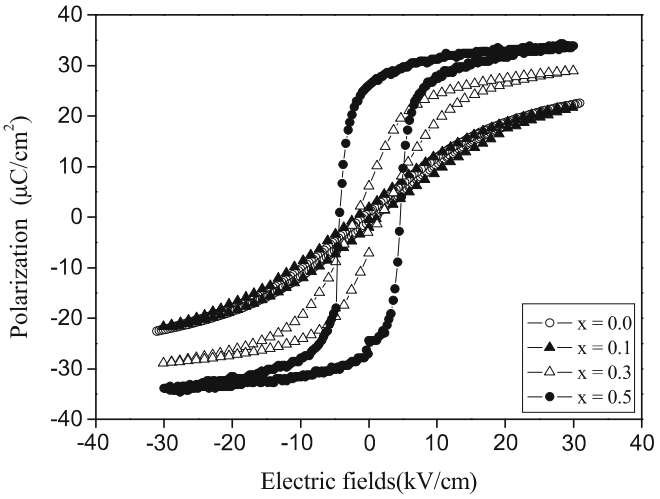

FIGURE 4 . (. −*x*) *x*

(−*x*) *x*

x

E /

P *x*

P *x* = .

. μ / . μ /

P

P (. μ /)

x = . B

(*T* ≈ °) (*T* ≈ °)

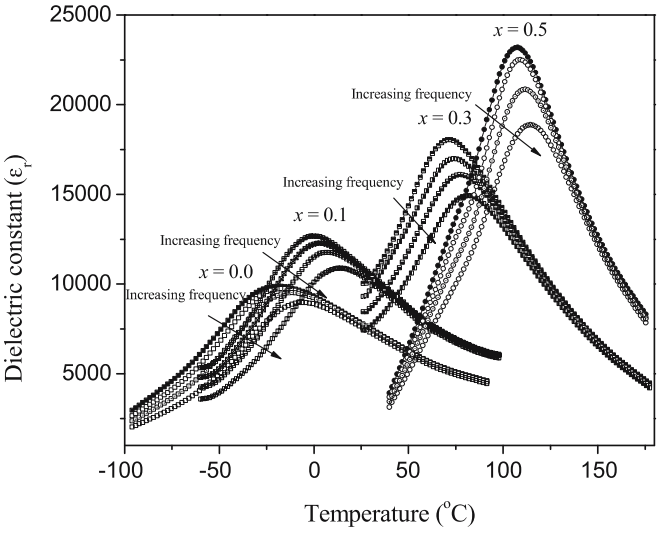

FIGURE 5 . (. −*x*) *x*

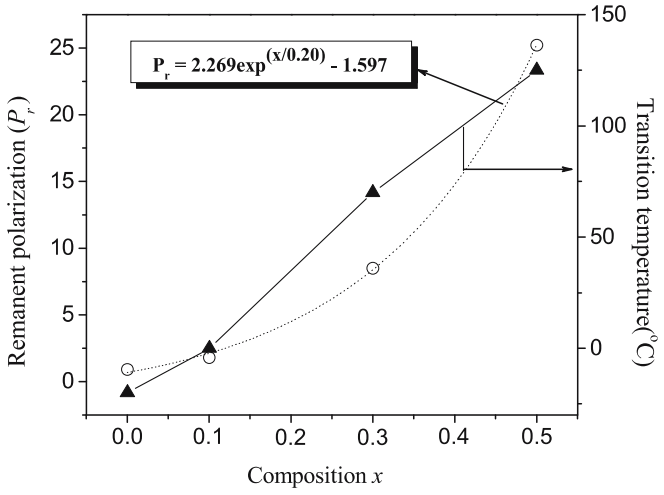

FIGURE 6
(. −x) x x

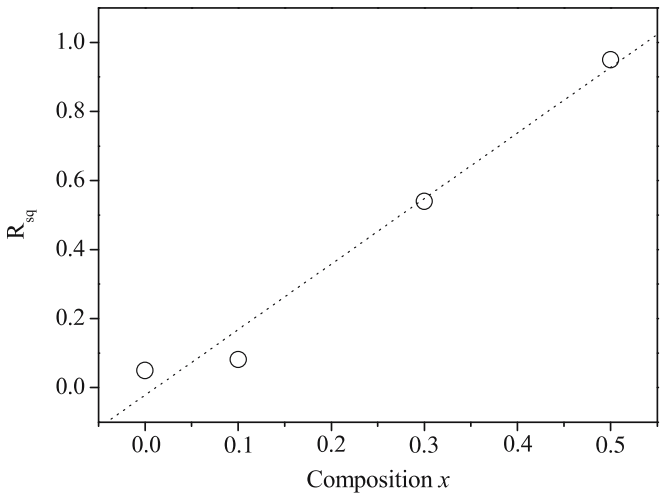

FIGURE 7 P E
. (. −x) x

x

T x
x

x A

P = . (x/ .) − . μ / ( )
(x)

$$R = \frac{P}{P} + \frac{P_{.E}}{P}, \qquad (\ )$$

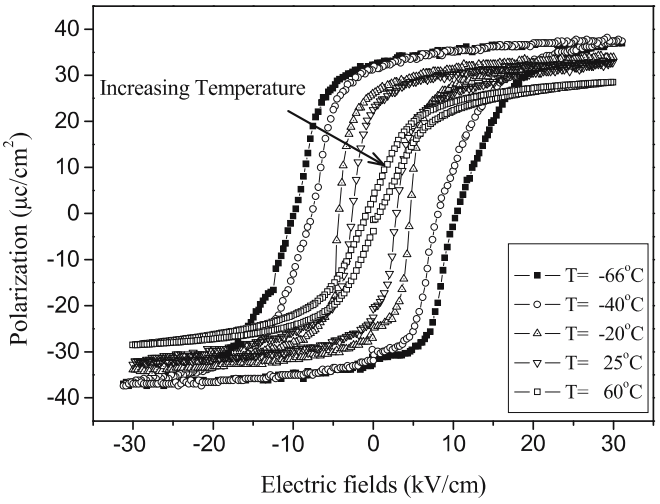

FIGURE 8 P E .
(. −x) x
x = .

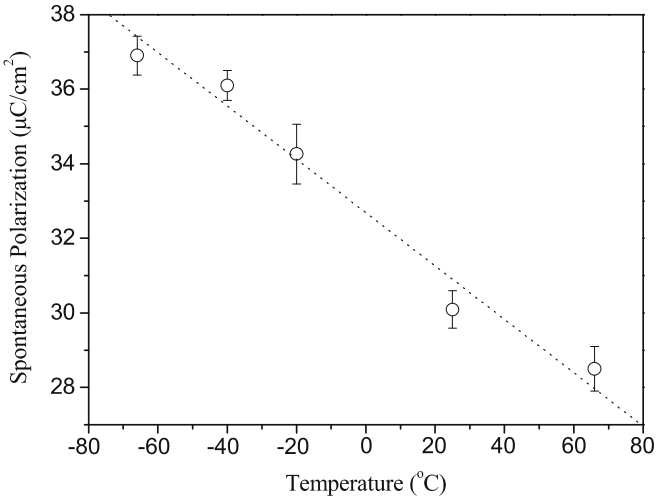

FIGURE 9 . (. −x) x
x = .

R P
P
P . E

x
R

x = .

x = .
− °

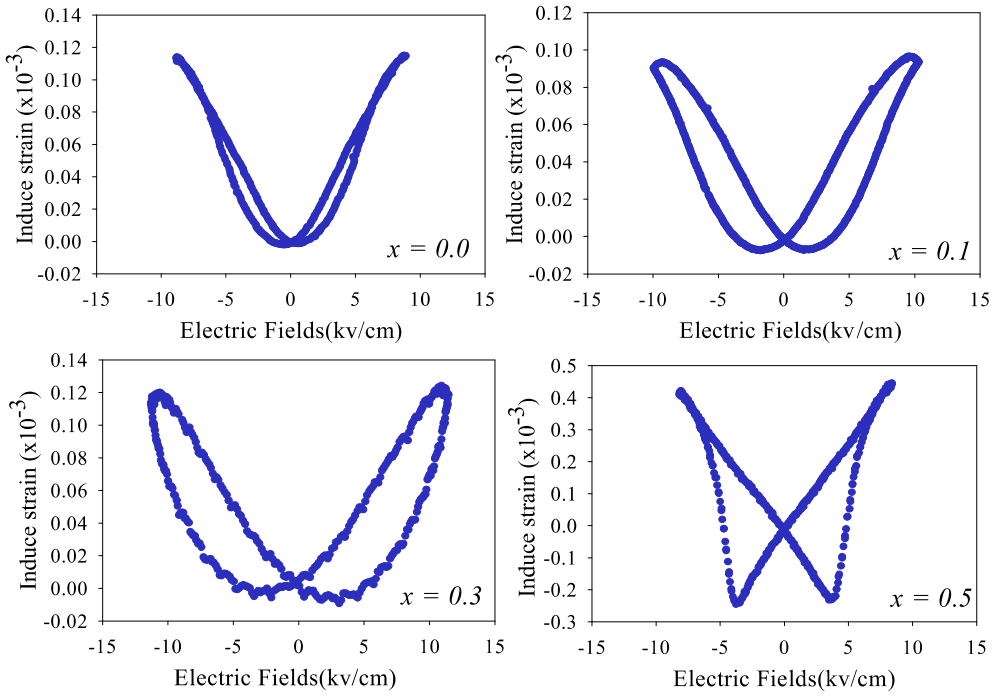

FIGURE 10

. (. –
x) *x*

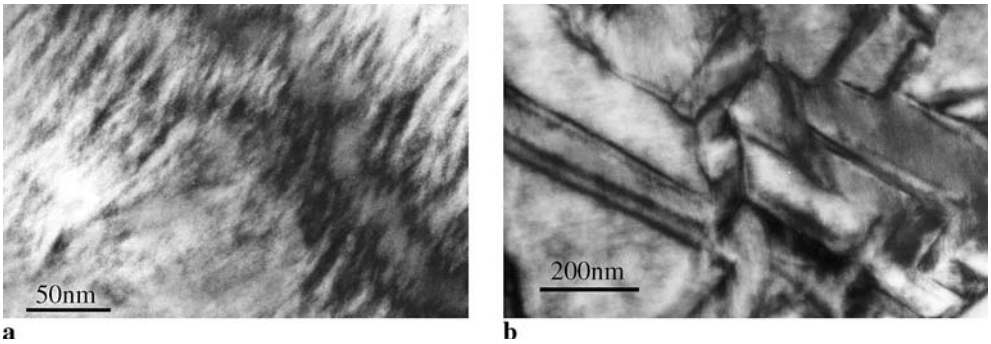

FIGURE 11

(a) *x* = . **(b)** *x* = .

(*x* = .)

ε *E*

x = .

A

P = . – . *x*, ( ) /

x A

x = .

3.3 *Microstructure characterization*

. (–
x) *x*

A

A *x* = .

x = .

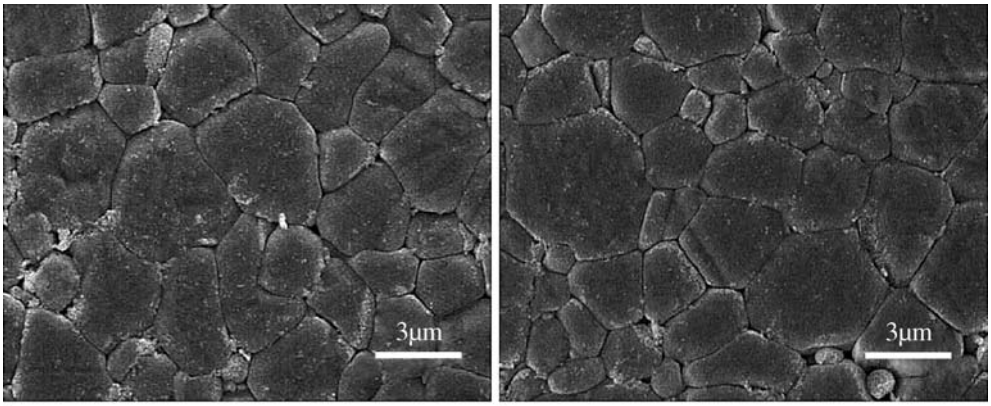

a b

FIGURE 12

. (. $-x$) x
(**a**) $x =$. (**b**) $x =$.

. (. $-x$) x $x =$.
$x =$. A
B

. μ

4 Conclusions

( ) /
(° /)

$x =$. P P
E . μ / . μ / . /

ACKNOWLEDGEMENTS

( )
(A)

REFERENCES

Ferroelectric Materials and Their Applications (
A)
Ferroelectric Devices ( )
151 ( )
A
16 ( )

A **6** ( )
A
A **96** ( )
A A A
A **81** ( )
A B A A *Proc. 11th Symp. Application of Ferroelectrics* A

Proc. 8th US–Japan Seminar on Dielectric and Piezoelectric Ceramics
A
A **77** ( )

B **108** ( )
Proc. 5th IEEE Int. Conf. Properties and Application of Dielectric Materials

71 ( )
B A A **65** ( )

Ferroelectrics
Publication details, including instructions for authors and subscription information:
http://www.informaworld.com/smpp/title~content=t713617887

Influence of Strontium Doping on the Ferroelectric and Piezoelectric Properties of Lead Zinc Niobate-Lead Zirconate Titanate Ceramics

Naratip Vittayakorn [a]; Theerachai Bongkarn [b]
[a] Department of Chemistry, Faculty of Science, King Mongkut's Institute of Technology, Ladkrabang, Bangkok, Thailand
[b] Department of Physics, Faculty of Science, Naresuan University, Pitsanuloke, Thailand

First Published on: 01 November 2007
To cite this Article: Vittayakorn, Naratip and Bongkarn, Theerachai (2007) 'Influence of Strontium Doping on the Ferroelectric and Piezoelectric Properties of Lead Zinc Niobate-Lead Zirconate Titanate Ceramics', Ferroelectrics, 358:1, 54 - 59
To link to this article: DOI: 10.1080/00150190701533967
URL: http://dx.doi.org/10.1080/00150190701533967

Ferroelectrics, 358:54–59, 2007

ISSN: 0015-0193 print / 1563-5112 online
DOI: 10.1080/00150190701533967

Taylor & Francis
Taylor & Francis Group

Influence of Strontium Doping on the Ferroelectric and Piezoelectric Properties of Lead Zinc Niobate-Lead Zirconate Titanate Ceramics

NARATIP VITTAYAKORN[1]
AND THEERACHAI BONGKARN[2,*]

[1]Department of Chemistry, Faculty of Science, King Mongkut's Institute of Technology, Ladkrabang, Bangkok 10520, Thailand
[2]Department of Physics, Faculty of Science, Naresuan University, Pitsanuloke 65000, Thailand

The crystal structure, ferroelectric and piezoelectric properties of pyrochlore-free lead zinc niobate-lead zirconate titanate ceramics were investigated systematically as a function of Sr doping as well as thermal treatment. The results showed that the remanent polarization (P_r) has decreased significantly with increase in strontium content. After annealing, the value of squareness of hysteresis loop (R_{sq}) increased from 1.48 to 1.74 for the annealed sample. Furthermore the annealed samples exhibited larger P_r and lower coercive fields (E_c) compared with as-sintered samples. The results indicated that the ferroelectric and piezoelectric properties in Sr-modified PZT-PZN were further improved by thermal annealing.

Keywords Thermal treatment; hysteresis loop; ferroelectric properties

Introduction

Lead zirconate titanate (PZT) occupies an important place in the field of ferroelectricity since the mid 1950s, as its properties can easily be tailored for specific applications by the addition of appropriate dopants or substituents [1, 2]. Recently, Zheng et al. [3] have reported that Sr-modified PZT ceramics generally have higher dielectric and piezoelectric properties than pure PZT. Sr substitutions on the A-site in PZT tended to shift the MPB composition toward the tetragonal phase.

Lead zinc niobate, $Pb(Zn_{1/3}Nb_{2/3})O_3$, (PZN) is a well known relaxor ferroelectric that has been noted for its high permittivity and extremely high piezoelectric coefficients [4]. It is known that perovskite PZN ceramics cannot be synthesized by the conventional mixed-oxide method without doping [5]. It is well known that replacement of the A-site ion (Pb) by an ion with a large radius such as Ba or Sr is also considered to be a good approach to stabilize the perovskite phase [5].

Recently our previous work [6, 7] observed large coupling coefficients and large piezoelectric constants in PZN-PZT ceramics. Work by Kim et al. [8] on PZN-PZT

Received September 3, 2006; accepted September 14, 2006.
*Corresponding author. E-mail: naratipcmu@yahoo.com

ceramics reported that a dielectric and piezoelectric properties were improved with increased annealing time. This study is concerned with the effect of Sr substituted PZT modified with the relaxor ferroelectric PZN. Special emphasis is placed on the piezoelectric and ferroelectric properties before and after thermal treatment. Based on our previous [6] results for the PZN-PZT system, PZT containing 30 mol% of PZN was selected as the starting composition which is close to the rhombohedral MPB in this system.

Experimental

The composition selected for the present study is $Pb_{(1-x)}Sr_x[0.7(Zr_{1/2}Ti_{1/2})$ $0.3(Zn_{1/3}Nb_{2/3})]O_3$, where $x = 0$–0.06. The mixture was calcined at 900°C for 4 h in air, remilled, pressed into disks ∼10.0 mm in diameter at around 80 MPa, and then sintered at 1200°C for 2 h in a sealed alumina crucible with a $PbZrO_3$ powder atmosphere. To determine the effect of thermal annealing, all of the sintered samples were thermally annealed at 900° C in the same PbO atmosphere for 24 h. The crystal structure of solid solutions was analyzed using X-ray diffractometry XRD (PW1729, Philips, Netherlands). The bulk density was measured using the Archimedes method. The piezoelectric constant (d_{33}) was measured using a quasi-static piezoelectric d_{33} meter (Model 8000 d_{33} Tester). The planar coupling coefficient (k_p) was determined by the resonance and anti-resonance technique using an impedance analyzer (Model HP4194A, Hewlett-Packard, CA). In addition, the polarization (P) was measured as a function of electric field (E), using a ferroelectric tester system (Radiant Technologies, Inc., PT66A).

Results and Discussions

Figure 1 shows the XRD diffraction patterns of $Pb_{(1-x)}Sr_x[0.7(Zr_{1/2}Ti_{1/2})$ $0.3(Zn_{1/3}Nb_{2/3})]O_3$, where $x = 0$–0.06 specimens, each exhibiting a phase-pure perovskite phase within the detection limit of the equipment. The XRD data is consistent with rhombohedral symmetry, which is indicative of a ferroelectric phase. With the peaks properly indexed, lattice parameter was determined using UnitCell, a linear least squares refinement program. The calculated lattice parameters of the perovskite structures and the densities of the as-sintered and annealed specimens containing different amounts of strontium are presented in Table 1. An increase in the mole faction of Sr^{2+} did not show any evidence of a change in symmetry. Also, the lattice constant linearly decreases with the replacement of Pb^{2+} by Sr^{2+} according to the Vegard rule. It indicates that, together with the XRD patterns in Fig. 1, complete series of perovskite solid solutions are formed. In general, the lattice parameters of the perovskite structure also decreased gradually as $x$increased, undoubtedly because of the introduction of the smaller strontium ion ($r = 1.27$ Å) into the lead site ($r = 1.49$ Å), resulting in decreasing of the unit cell. The densification behavior of the specimen was greatly influenced by the strontium content. The density decreased almost linearly with increasing strontium concentration for both of the samples. Figure 2(a) and (b) display the hysteresis curves of doped PZT-PZN samples in the as-sintered state (Fig. 2(a)) and after annealing (Fig. 2(b)). As one can expect the polarization decreased with increasing Sr dopant concentration.

Haertling and Zimmer [9] derived an empirical relationship between remanent polarization, saturation polarization and polarization at fields above the coercive field. This permits the quantification of changes in the hysteresis behavior for each sample through the

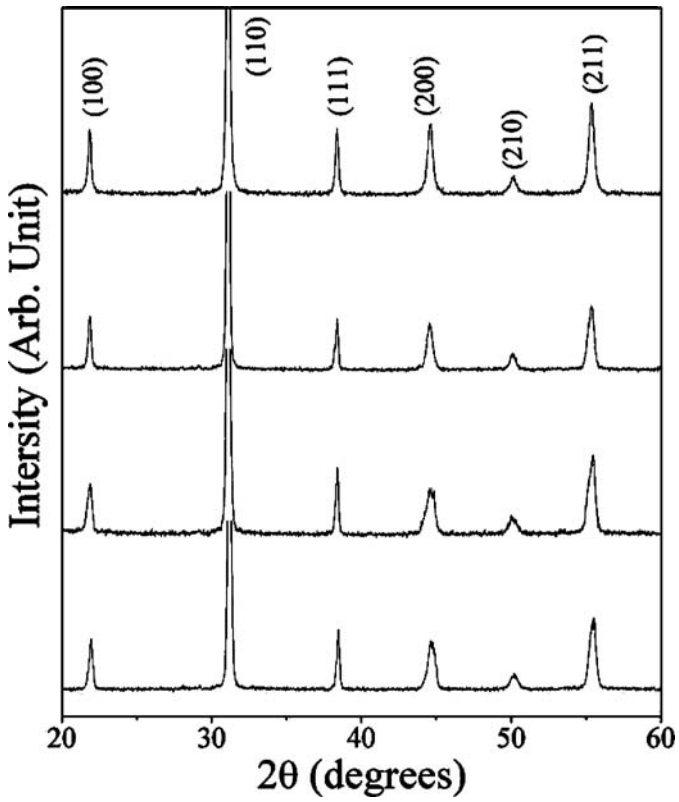

Figure 1. XRD patterns of $Pb_{(1-x)}Sr_x[0.7(Zr_{1/2}Ti_{1/2})\ 0.3(Zn_{1/3}Nb_{2/3})]O_3$, where $x = 0$-0.06 ceramic samples sintered at different temperatures.

following equation:

$$R_{sq} = \frac{P_r}{P_s} + \frac{P_{1.1Ec}}{P_r} \tag{1}$$

where, R_{sq} is the squareness of hysteresis loop, P_r is remanent polarization, P_s is saturation polarization, $P_{1.1}E_c$ is the polarization at an electric field equal to 1.1 times the coercive field

Table 1
Physical characteristic of $Pb_{(1-x)}Sr_x[0.7(Zr_{1/2}Ti_{1/2})\ 0.3(Zn_{1/3}Nb_{2/3})]O_3$, where $x = 0$–0.06 ceramics

		Density(g/cm^3)	
Composition	Lattice parameter (Å)	As-sintered	Annealed
$x = 0.0$	4.0642 ± 0.008	7.71 ± 0.05	7.82 ± 0.06
$x = 0.02$	4.0568 ± 0.009	7.64 ± 0.03	7.76 ± 0.03
$x = 0.04$	4.0556 ± 0.012	7.58 ± 0.03	7.68 ± 0.08
$x = 0.06$	4.0462 ± 0.011	7.47 ± 0.06	7.54 ± 0.04

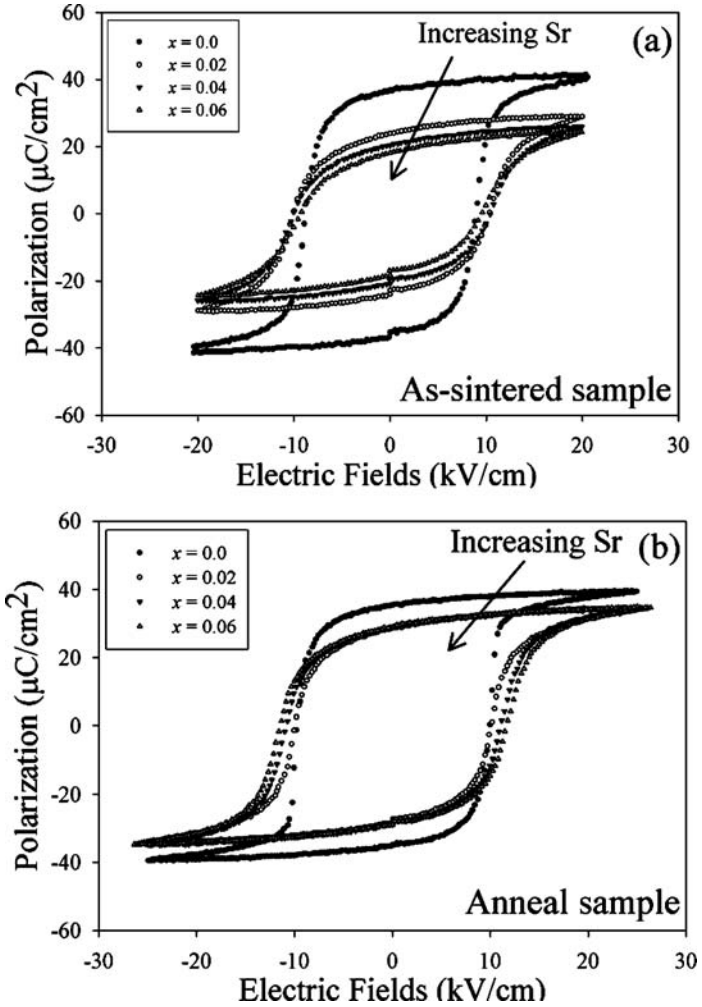

Figure 2. Dependence of the polarization versus electric field (P-E) loop on the Sr dopant concentration (a) as-sintered (b) anneal sample.

(E_C). For an ideal hysteresis loop, the squareness parameter is equal to two. Normal square ferroelectric P-E loops were observed in undoped as-sintered samples. After annealing, the value of R_{sq} increased from 1.48 to 1.74 for the annealed sample. In the as-sintered samples, the hysteresis curves also become more slanted with increasing Sr content. The remanent polarization decreased from 31.9 μC/cm^2 to 20.2 μC/cm^2 for the sample doped with 0.04 mol Sr.

However the coercive field increased from 10.6 kV/cm to 12.7 kV/cm after doping with 0.06 mol Sr. Furthermore the annealed samples exhibited larger remnant polarizations (P_r) and lower coercive fields (E_c) compared with as-sintered samples, which mean that the annealed ceramic samples are more easily poled and should have better piezoelectric properties. It is interesting to note that in annealed samples, the value of P_r was largely independent of the doping concentration and amounts to approximately 29 μC/cm^2. However the coercive fields were found to increase with increasing Sr concentration. Figure 3(a)

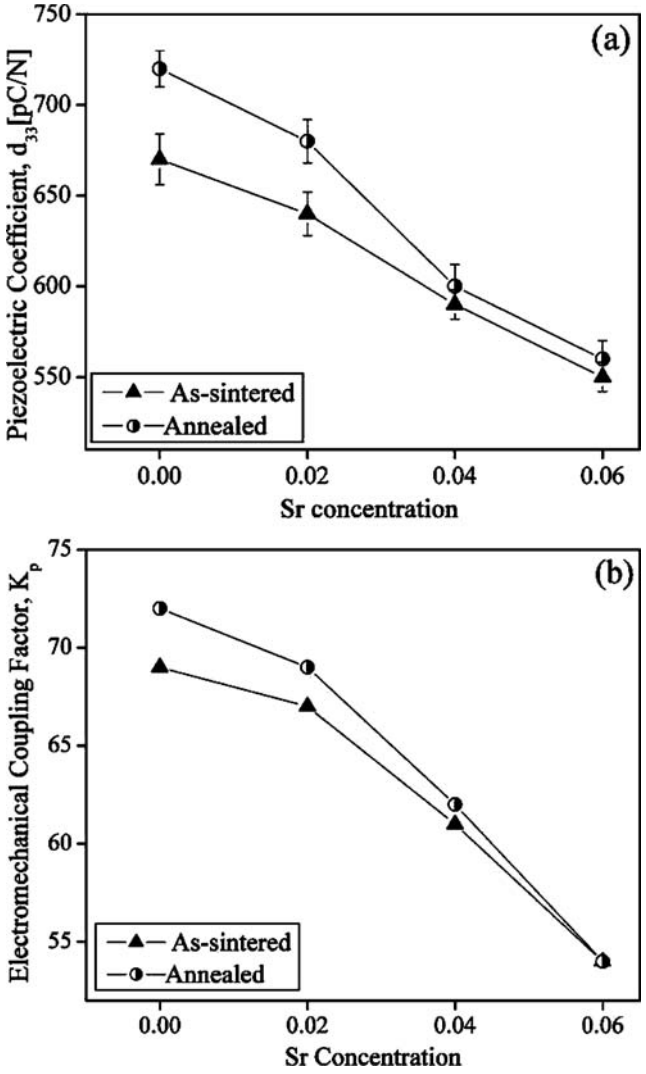

Figure 3. Electromechanical coupling factor and piezoelectric constant (d_{33}) of PZT-PZN specimens with Sr doping concentration.

and (b) shows the changes in the piezoelectric constant (d_{33}) and the electromechanical coupling factor (k_p) as a function of the amount of Sr addition. As can be seen, both k_p and d_{33} show a similar variation with increasing Sr content. The piezoelectric constant (d_{33}) and the electromechanical coupling factor (k_p) decreases with increasing Sr content .After annealing at 900°C for 24 h, d_{33} increases from 670 to 720 pC/N, and k_p increases from 69% to 72% for 0.7PZT-0.3PZN, while there is only a slight change in k_p and d_{33} for 6 mol% Sr-doped PZT-PZN.

Conclusions

The ferroelectric properties of Sr-modified PZT-PZN ceramics formed via the columbite process were investigated. The lattice parameters of the perovskite structure decreased

gradually as x increased, undoubtedly because of the introduction of the smaller strontium ion into the lead site. The best ferroelectric properties were attained in the annealed samples. Furthermore, the piezoelectric constant (d_{33}) and the electromechanical coupling factor (k_p) decreases with increasing Sr content in the annealed samples.

Acknowledgments

This work was supported by the Thailand Research Fund (TRF), Commission on Higher Education (CHE), Office of the National Research Council of Thailand (NRCT) and King Mongkut's Institute of Technology Ladkrabang.

References

1. B. Jaffe and W. R. Cook, Piezoelectric ceramic (R.A.N. Publishers, 1971).
2. K. Uchino, Ferroelectric Devices (Marcel Dekker, Inc., New York, 2000).
3. H. Zheng, I. M. Reaney, W. E. Lee, N. Jones, and H. Thomas, *J. Eur. Ceram. Soc*. **21**, 1371–1375 (2001).
4. Y. Yokomizo, T. Takahashi, and S. Nomura, *J. Phys. Soc. Jpn.* **28**, 1278–1284 (1970).
5. T. R. Shrout and A. Halliyal, *Am. Ceram. Soc. Bull*. **66**, 704 (1987).
6. N. Vittayakorn, G. Rujijanagul, T. Tunkasiri, X. Tan, and D. P. Cann, *Mat. Sci. Eng*. **B108**, 258 (2004).
7. N. Vittayakorn, C. Puchmark, G. Rujijanagul, X. Tan, and D. P. Cann, *Current Applied Physics* **6**, 303–306 (2006).
8. H. Fan and H.-E. Kim, *J. Appl. Phys*. **91**, 317 (2002).
9. G. H. Haertling and W. J. Zimmer, *Am. Ceram. Soc. Bull.* **45**, 1084 (1966).

Phase transitions and ferroelectric properties in $BiScO_3$-$Bi(Zn_{1/2}Ti_{1/2})O_3$-$BaTiO_3$ solid solutions

Chien-Chih Huang[a] and David P. Cann
Materials Science, Department of Mechanical Engineering, Oregon State University, Corvallis, Oregon 97331

Xiaoli Tan
Materials Science and Engineering Department, Iowa State University, Ames, Iowa 50011

Naratip Vittayakorn
Department of Chemistry, King Mongkut's Institute of Technology Ladkrabang, Bangkok, Thailand 10520

(Received 9 May 2007; accepted 1 July 2007; published online 21 August 2007)

Ceramics solid solutions within the ternary perovskite system $Bi(Zn_{1/2}Ti_{1/2})O_3$-$BiScO_3$-$BaTiO_3$ were synthesized via solid-state processing techniques. The crystal structure of sintered ceramics was analyzed by x-ray diffraction. A stable perovskite phase was obtained for all compositions with a $BaTiO_3$ content greater than 50 mol %. Furthermore, a change in symmetry from pseudocubic to tetragonal was observed as the mole fraction of $BaTiO_3$ increased. Dielectric measurements show a dielectric anomaly associated with a phase transformation over the temperature range of 30 °C–210 °C for all compositions. Examination of the polarization hysteresis behavior revealed weakly nonlinear hysteresis loops. With these data, ferroelectric phase diagrams were derived showing the transition between the pseudocubic relaxor behavior to the tetragonal normal ferroelectric behavior. This transition was also correlated with changes in the diffuseness parameter. © *2007 American Institute of Physics*. [DOI: 10.1063/1.2769787]

I. INTRODUCTION

Perovskite $Pb(Zr,Ti)O_3$ (PZT) ceramics are widely used for many industrial applications due to their superior performance in piezoelectric, dielectric, and pyroelectric applications. However, recently there have been environmental concerns about PZT related to the toxicity of lead oxides which are volatile during processing. Consequently, this has motivated the search for lead-free piezoelectric materials with piezoelectric properties comparable to PZT with a reduced environmental impact.

The origin of the enhanced piezoelectric response in perovskite PZT is the result of lone pair electrons in the Pb^{2+} hybrid orbitals[1] and the existence of a morphotropic phase boundary (MPB) between two ferroelectric phases.[2] Therefore, Bi^{3+} is an excellent candidate for the substitution of Pb in the PZT system since it has a similar electronic structure and there are already numerous Bi-based perovskite ceramics that can be used in solid solutions.[3–8] Through systematic research, a number of MPB systems based on $Bi(M)O_3$-$PbTiO_3$ ($M=Ti^{4+}$, Sc^{3+}, Zn^{2+}, Nb^{5+},…) have been discovered.[6,8] Recently, $BiScO_3$ (BS) perovskite has drawn attention due to its high Curie temperature ($T_c=450$ °C) and its excellent piezoelectric properties at the MPB with $PbTiO_3$.[6] Another Bi-based perovskite, $Bi(Zn_{1/2}Ti_{1/2})O_3$, exhibits a high T_c with an enhanced tetragonality through solid solution with $PbTiO_3$.[8,9] However, both $BiScO_3$ and $Bi(Zn_{1/2}Ti_{1/2})O_3$ are unstable in their pure form and can only be stabilized under high pressures[10,11] or in solid solutions with other perovskite end members.[6,8] In order to develop lead-free piezoelectric materials, $BaTiO_3$ (BT) was used for this research in order to stabilize the BZT and BS perovskite phases in a solid solution.

Recently, Tinberg *et al.* reported ferroelectric thin films based on the $BiScO_3$-$BaTiO_3$ binary system.[12] Similar to the $BiScO_3$-$PbTiO_3$ system, when $PbTiO_3$ was replaced with $BaTiO_3$, the perovskite structure was stabilized and a MPB was observed. Although there are no reports related to the $Bi(Zn_{1/2}Ti_{1/2})O_3$-$BaTiO_3$ system, an increased transition temperature can be expected for this system.

In this work, the phase equilibria and dielectric properties of the ternary solid solution $BiScO_3$-$Bi(Zn_{1/2}Ti_{1/2})O_3$-$BaTiO_3$ (BS-BZT-BT) were examined. This article may provide an alternative approach for lead-free piezoelectric materials development.

II. EXPERIMENTAL PROCEDURE

Solid solutions of $(1-x)(0.5BiScO_3$-$0.5Bi(Zn_{1/2}Ti_{1/2})O_3)$-$xBaTiO_3$ (BS-BZT-BT) were prepared by conventional ceramic processing. Reagent grade oxide powders of Bi_2O_3(≥99.9%), ZnO(≥99%), TiO_2(≥99.9%), and $BaCO_3$(≥99.5%) were batched in stoichiometric amounts and ball-milled with ethanol and yttrium-stabilized zirconia media for 6 h. The dried powders were double calcined in open crucibles between 800 °C–950 °C for 24 h and followed by an additional milling and drying step. The calcined powders were mixed with 3 wt % polyvinyl alcohol (PVA) and then uniaxially cold-pressed at 150 MPa into 12.7 mm diameter pellets. Following binder burnout at 500 °C, the pellets were sintered in sealed crucibles between 850 °C–1200 °C for 2 h. For phase determination, x-ray

[a]Electronic mail: huangch@onid.orst.edu

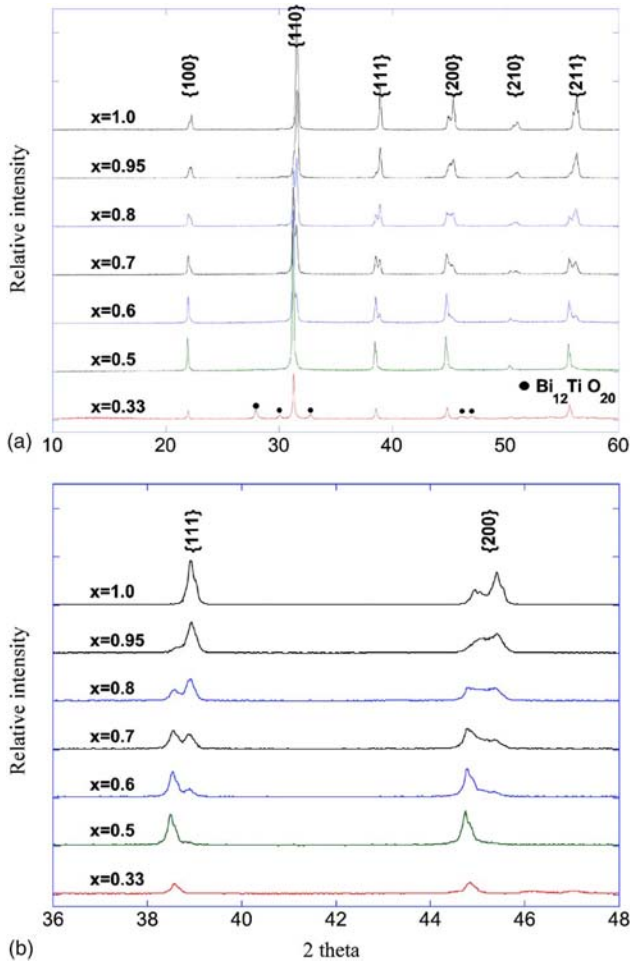

FIG. 1. (Color online) XRD diffraction pattern of calcined $(1-x)$(BS-BZT)-xBT powders.

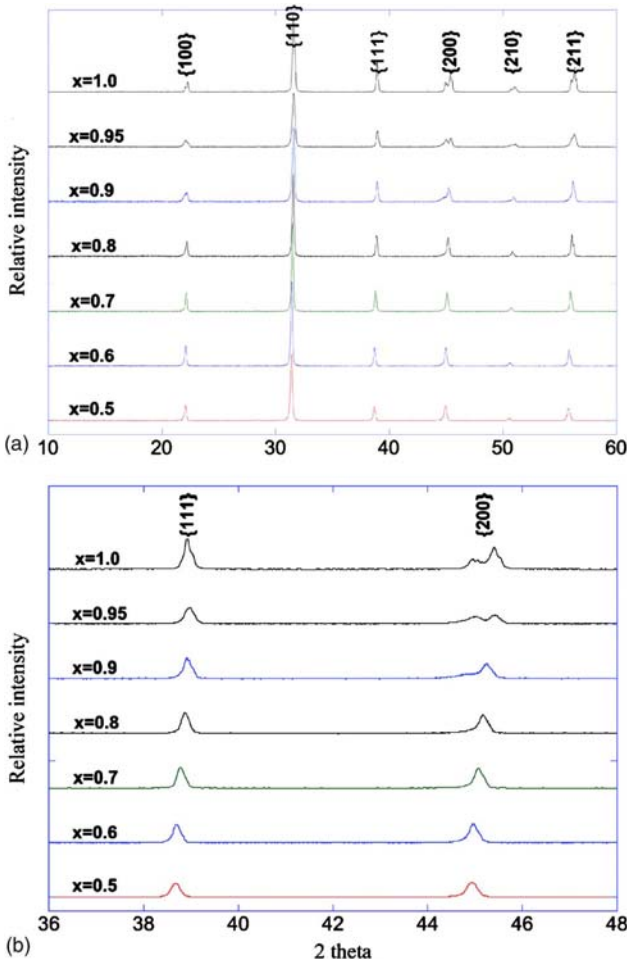

FIG. 2. (Color online) XRD diffraction pattern of sintered $(1-x)$(BS-BZT)-xBT ceramics.

diffraction (XRD, Siemens D5000 diffractometer) was utilized in the 2θ scan range of $10-60°$ for calcined powders and sintered pellets.

Prior to the electrical measurements, the pellets were polished to smooth and parallel surface. After polishing, a silver electrode paste (Heraeus C1000) was applied and then fired at 600 °C. An Agilent 4284A LCR was used to measure the dielectric properties over a wide temperature range using a NorECS ProboStat high-temperature measurement cell. The polarization versus electric field hysteresis loops of selected compositions were recorded at room temperature and −50 °C, respectively, with a RT66A standard ferroelectric test system (Radiant Technologies).

III. RESULTS AND DISCUSSION

A. Perovskite phase determination

Figure 1(a) displays the XRD patterns for calcined powders of $(1-x)$(BS-BZT)-xBT. Perovskite phases were obtained for compositions containing at least 50 mol % $BaTiO_3$. For compositions below this amount, a complex mixture of phases was observed. Based on the {111} and {200} peak splittings shown in Fig. 1(b), the composition with $x=0.5$ corresponds to a pure rhombohedral symmetry. Compositions above $x=0.95$ stabilized in a pure tetragonal symmetry. The peaks between these two compositions indicated the coexistence of rhombohedral and tetragonal phases. The XRD patterns of sintered $(1-x)$(BS-BZT)-xBT pellets shown in Fig. 2 confirm that the samples retained phase pure perovskite for all compositions with 50 mol % and above $BaTiO_3$. In contrast to the calcined powders, in the sintered pellets the tetragonal perovskite phase was only present for compositions with $x=0.95$ to $x=1$. The remainder of the compositions $x\leq 0.9$ exhibited a rhombohedral symmetry. These results indicate that the MPB in this system may be located between $x=0.9$ and 0.95. This shift in symmetry between the calcined and sintered samples may be due to a number of factors. The observation of the coexistence of two perovskite phases in calcined powders is likely the result of the relatively low processing temperature. The limited reaction kinetics may have resulted in an incomplete reaction between BT, BS, and BZT. In addition, both Bi_2O_3 and ZnO have some degree of volatility at this temperature that may have caused a slight change in composition. Upon sintering, homogenization occurred, leading to a clearly observed single-perovskite phase.

The lattice parameters were calculated from XRD patterns shown in Table I. Although Bi^{3+} is slightly smaller than

TABLE I. Room-temperature structure and dielectric data for all compositions at 10 KHz.

x mol % BT	0.5	0.6	0.7	0.8	0.9	0.92	0.95	1
Structure	Rhombohedral						Tetragonal	
lattice parameter (Å)	4.046	4.040	4.030	4.022	4.014	4.009	a: 3.997 c: 4.023	a: 3.992 c: 4.034
T_m(°C)	208	161	118	76	45	33	111	134
ε_m at T_m	1100	1170	1240	1360	2570	3960	3520	9740
δ	587.5	210.3	143.1	70	61.4	57.3	16.3	3.4
γ	1.99	1.74	1.65	1.67	1.66	1.44	1.38	1.11

Ba^{2+} based on 12-fold coordination, the unit cell volume increased with decreasing $BaTiO_3$ content due to substitution of larger size B-site cations Zn^{2+}(0.88 Å) and Sc^{3+}(0.885 Å) for Ti^{4+}(0.745 Å). Comparing the tetragonal structure for $x=1$ and $x=0.95$, the results show that the $c:a$ ratio increased with $BaTiO_3$ content. This may be due to the phase transition for $x=0.95$ that occurs close to room temperature, which results in the formation of a pseudocubic phase.

B. Dielectric behavior of BS-BZT-BT

The dielectric constant and dielectric loss were measured from 100 Hz to 100 KHz as a function of temperature. The room-temperature dielectric properties for all of the compositions in this study are listed in Table I. Figure 3 shows the

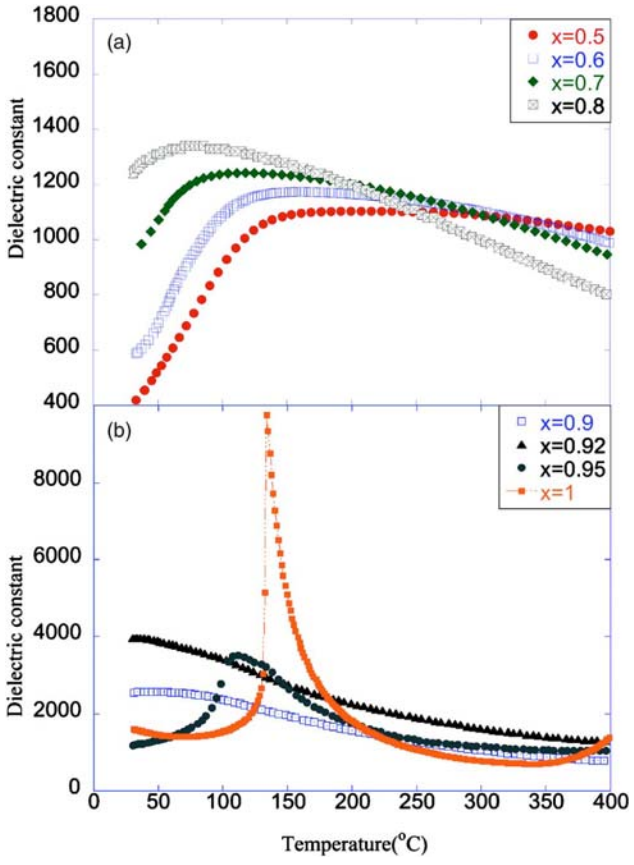

FIG. 3. (Color online) Dielectric constant of $(1-x)$(BS-BZT)-xBT as a function of temperature at measuring frequency of 10 kHz.

permittivity versus temperature at 10 KHz for $(1-x)$(BS-BZT)-xBT from $x=0.5$ to 1.0. It was observed that the maximum permittivity, ε_m, increased with increasing $BaTiO_3$ content. However, temperature at which maximum permittivity appeared, T_m, exhibited a more complex trend. It is very clear from the data that, while pure $BaTiO_3$ exhibited a strong first-order phase transition, the addition of BS+BZT caused a shift toward relaxor ferroelectric behavior. It is well known that perovskite $BaTiO_3$ has three phase transitions within a wide range of temperature.[13] According to our XRD data in Fig. 2, when mixed with more than 10 mol % BS-BZT, all three transition temperatures merged into one diffuse transition which is also reflected in the XRD data. This kind of phenomenon has also been noted when $BaTiO_3$ was mixed with $BaZrO_3$.[14] In Table I, the data clearly show that T_m decreased with increasing $BaTiO_3$ content for $x \leq 0.9$. On the contrary, T_m increased with $BaTiO_3$ content for $x \geq 0.95$.

For a diffuse phase transition, the degree of diffuseness can be obtained from the parameter δ_r derived via the following expression:[15]

$$\frac{\varepsilon'_m}{\varepsilon'(f,T)} = 1 + \frac{[T - T_m(f)]^\gamma}{2\delta_\gamma^2} (1 \leq \gamma \leq 2). \quad (1)$$

The parameter of γ is degree of dielectric relaxation, where $\gamma=1$ corresponds to a normal first-order ferroelectric phase transition. Larger values of γ express more relaxor-ferroelectric behavior of transition. The value of δ_r represents degree of diffuseness for transition peaks. Both γ and δ_r were determined from the slope and intercept of $\ln(\varepsilon'_m/\varepsilon')$ vs $\ln(T-T_m)$. According to Table I, a greater percentage of BS and BZT resulted in a higher degree of diffuseness and stronger relaxor behavior. This can be explained by the increased cation disorder due to the substitution on the A-site by Bi and on the B-site by Sc and Zn.

The dielectric property as a function of frequency for $(1-x)$(BS-BZT)-xBT is shown in Fig. 4. A strong frequency dependence characteristic of a relaxor ferroelectric was observed. The peaks appearing around 600 °C for $x=0.8$ are likely the result of oxygen vacancies.[16] Moreover, these compositions possess a stable dielectric constant of approximately 1000 and low loss tangent ($\tan\delta < 0.01$) up to high temperatures ($T < 400$ °C). It may have great potential for high-temperature applications.

The polarization versus electric field measurements at 4 Hz for $x=0.5$ and $x=0.7$ are shown in Fig. 5. The samples used in this study were sintered without being covered,

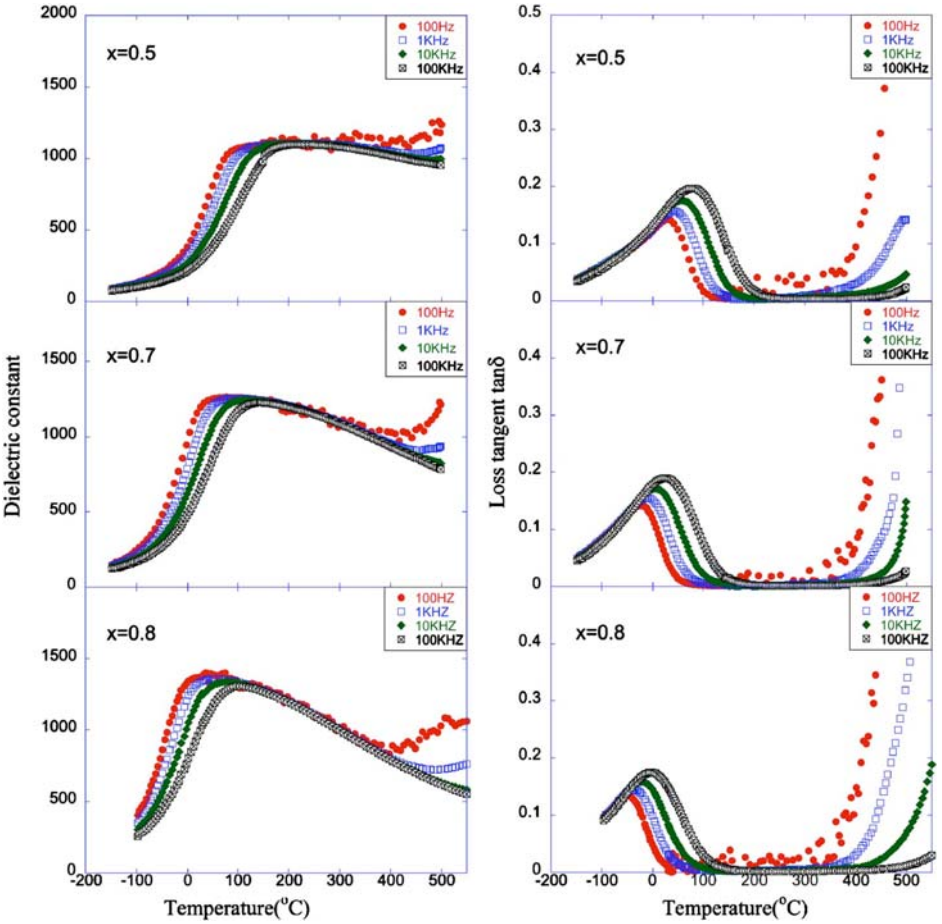

FIG. 4. (Color online) Dielectric constant and loss tangent of $(1-x)$(BS-BZT)-xBT with $x=0.5$, 0.7, and 0.8 as a function of temperature.

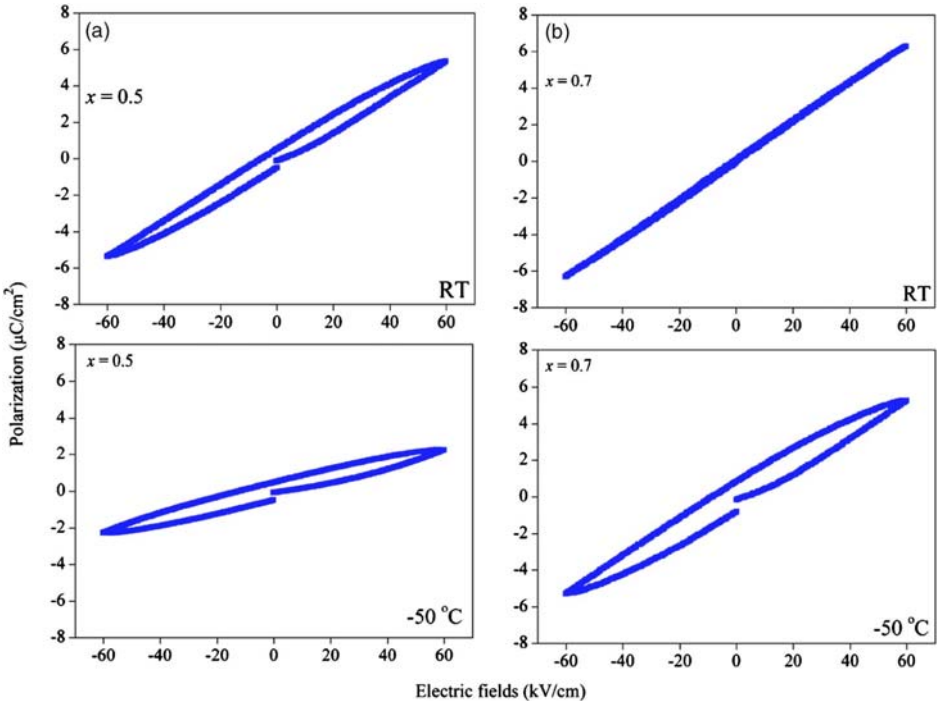

FIG. 5. (Color online) Polarization data on $(1-x)$(BS-BZT)-xBT ceramics at 4 Hz for (a) $x=0.5$ and (b) $x=0.7$.

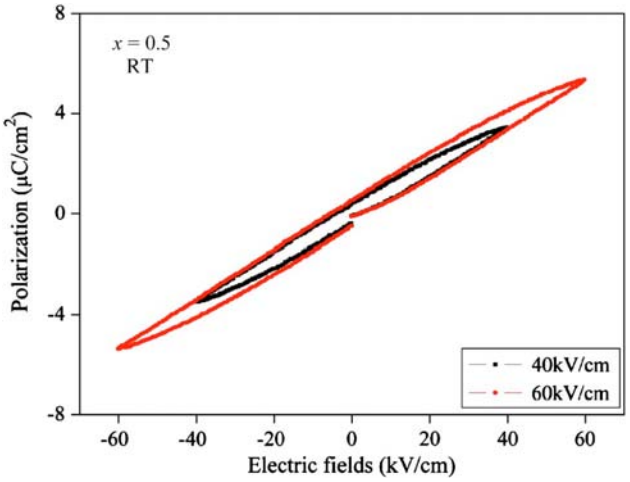

FIG. 6. (Color online) The *P-E* hysteresis loop measured from the ceramic of $x=0.5$ at 4 Hz at room temperature.

which, due to the loss of Zn and Bi, resulted in a slight downward shift in T_{max} (i.e., on the order of 10 °C–20 °C. The loop from the ceramic of $x=0.5$ exhibits a weak nonlinearity at room temperature, which is not unexpected given that the measurements were taken at a temperature in the vicinity of T_m. At $T=-50$ °C the slope of the loop decreased as expected due to the decrease in dielectric permittivity below T_m. Figure 6 displays room-temperature *P-E* data for $x=0.5$ as a function of electric field. As the *E*-field increases, a clear elliptical rotation is observed which is another indication of nonlinear behavior. The $x=0.7$ sample exhibited a narrow, weakly nonlinear loop at room temperature which broadened at lower temperatures corresponding to the increased tan δ below the transition temperature (Fig. 4). It is interesting to note that even at relatively high fields up to 60 kV/cm all the loops were weakly nonlinear with relatively low polarization values.

C. Phase transformations in the $(1-x)$(BS-BZT)-xBT system

Figure 7 presents data on the phase transformation in the $(1-x)$(BS-BZT)-xBT system obtained from the dielectric data. Starting from pure $BaTiO_3$ the phase transition decreases as the (BS-BZT) content increases to a minimum of 33 °C at $x=0.92$. At higher (BS-BZT) concentrations the transition temperature then increases up to $x=0.5$. Also plotted in Fig. 7 is the diffuseness parameter δ as a function of composition. Pure $BaTiO_3$ exhibits a sharp first-order phase transition, but as the (BS-BZT) content increases a quasilinear increase in δ is observed owing to increased relaxor behavior.

IV. CONCLUSION

Single-phase perovskite was obtained for $(1-x)$(BS-BZT)-xBT for compositions containing at least 50 mol % $BaTiO_3$. The XRD data revealed that a MPB may exist between 5–10 mol % BS-BZT added to $BaTiO_3$. The dielectric characterization revealed that as BS-BZT was added to $BaTiO_3$ the phase transition became very diffuse. The relaxor ferroelectric behavior was likely due to complex cation ordering on the *A*-site and on the *B*-site. Due to the diffuseness of the phase transition, the compositions in this study exhibited a very stable dielectric constant greater than 1000 and low loss tangents (<0.01) over a wide range of temperature ($T<400$ °C).

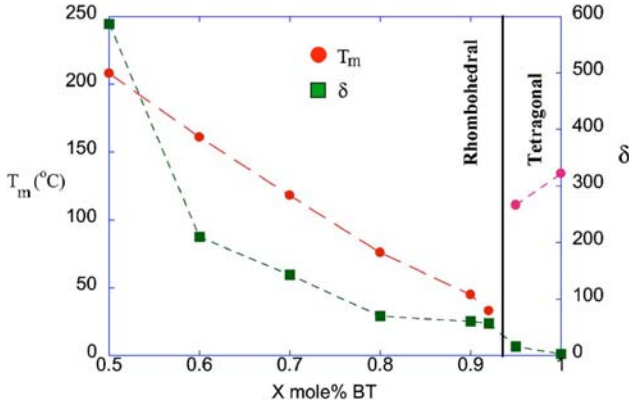

FIG. 7. (Color online) T_{max} and diffuseness δ as a function of $BaTiO_3$ content.

ACKNOWLEDGMENTS

The authors would like to thank Professor Doug Keszler for assisting with the XRD experiments, as well as Xiaohui Zhao for his assistance with the *P-E* measurements.

[1] R. E. Cohen, Nature **358**, 136 (1992).
[2] R. Guo, L. E. Cross, S.-E. Park, B. Noheda, D. E. Cox, and G. Shirane, Phys. Rev. Lett. **84**, 5423 (2000).
[3] C. F. Buhrer, J. Chem. Phys. **36**, 798 (1962).
[4] T. Takenaka, K. Maruyama, and K. Sakata, Jpn. J. Appl. Phys., Part 1 **30**, 2236 (1991).
[5] A. Sasaki, T. Chiba, Y. Mamiya, and E. Otsuki, Jpn. J. Appl. Phys., Part 1 **38**, 5564 (1999).
[6] R. E. Eitel, C. A. Randall, T. R. Shrout, P. W. Rehrig, W. Hackenberger, and S. -E. Park, Jpn. J. Appl. Phys., Part 1 **40**, 5999 (2001).
[7] M. R. Suchomel and P. K. Davies, J. Appl. Phys. **96**, 4405 (2004).
[8] M. R. Suchomel and P. K. Davies, Appl. Phys. Lett. **86**, 262905 (2005).
[9] I. Grinberg, M. R. Suchomel, W. Dmowski, S. E. Mason, H. Wu, P. K. Davies, and A. M. Rappe, Phys. Rev. Lett. **98**, 107601 (2007).
[10] Y. Y. Tomashpol'skii, E. V. Zubova, K. P. Burdina, and Y. N. Venevtsev, Sov. Phys. J. **13**, 859 (1969).
[11] M. R. Suchomel, A. M. Fogg, M. Allix, H. Niu, J. B. Claridge, and M. J. Rosseinsky, Chem. Mater. **18**, 4987 (2006).
[12] D. S. Tinberg and S. Trolier-McKinstry, J. Appl. Phys. **101**, 024112 (2007).
[13] B. Jaffe, W. Cook, and H. Jaffe, *Piezoelectric Ceramics* (Academic, London, 1971).
[14] Z. Yu, C. Ang, R. Guo, and A. S. Bhalla, J. Appl. Phys. **92**, 1489 (2002).
[15] A. A. Bokov and Z.-G. Ye, Solid State Commun. **116**, 105 (2000).
[16] B. S. Kang and S. K. Choi, Solid State Commun. **121**, 441 (2002).

Available online at www.sciencedirect.com
ScienceDirect
Current Applied Physics 8 (2008) 88–92
Current Applied Physics
An official journal of the KPS
www.elsevier.com/locate/cap
www.kps.or.kr

Influence of fabrication processing on phase transition and electrical properties of $0.8Pb(Zr_{1/2}Ti_{1/2})O_3$–$0.2Pb(Ni_{1/3}Nb_{2/3})O_3$ ceramics

G. Rujijanagul [a,*], N. Vittayakorn [b]

[a] Department of Physics, Faculty of Science, Chiang Mai University, Chiang Mai 50200, Thailand
[b] Department of Chemistry, Faculty of Science, King Mongkut's Institute of Technology, Ladkrabang, Bangkok 10520, Thailand

Received 9 January 2007; received in revised form 11 May 2007; accepted 21 May 2007
Available online 31 May 2007

Abstract

The binary system of $0.8Pb(Zr_{1/2}Ti_{1/2})O_3$–$0.2Pb(Ni_{1/3}Nb_{2/3})O_3$ ceramics were synthesized by conventional mixed oxide and columbite method. X-ray diffraction analysis demonstrated the coexistence of both the rhombohedral and tetragonal phases for the columbite prepared sample. Rhombohedral to tetragonal phase transition for columbite method was different compared with those of the mixed oxide method. The permittivity shows a shoulder at the rhombohedral to tetragonal phase transition temperature $T_{Rho-Tetra} = 195$ °C, and then a maximum permittivity (36,000 at 10 kHz) at the transition temperature $T_m = 277$ °C on ceramics prepared with the columbite method. However, piezoelectric coefficient (d_{33}) was measured to be 282 pC/N for the conventional method and higher than the columbite method. The results were related to the phase compositions and porosity of the ceramics.

PACS: 77.22.−d; 77.22.Gm; 77.84.Dy

Keywords: Phase transition; Dielectric properties; Ferroelectric properties; Columbite method

1. Introduction

$Pb(Ni_{1/3}Nb_{2/3})O_3$ (PNN) is a relaxor ferroelectric material which has a cubic structure at room temperature. It shows a broad dielectric peak near $T_c \approx -120$ °C with relative permittivity near 4000 at 1 kHz [1]. Nanometer-level chemical heterogeneity in the form of short range ordering of Ni^{2+} and Nb^{5+} on the B′ site was proposed to account for the diffuse phase transition [2]. Pure perovkite phase of PNN can be prepared by the columbite method. This material can be alloyed with normal ferroelectric to optimize the electrical properties [3].

Lead zirconate-titanate, $Pb(Zr_xTi_{1-x})O_3$ (PZT) is a normal ferroelectric material which has been extensively investigated in the past because of their owing to the exceptionally good dielectric and piezoelectric properties as well as high Curie temperature (>350 °C) [4]. The high dielectric and piezoelectric of PZT was found for the composition close to the morphotropic phase boundary (MPB). This MPB is located around $PbZrO_3$:$PbTiO_3 \sim 0.52$:0.48 and separates the Ti-rich tetragonal phase from the Zr-rich rhombohedral phase [4]. PZT-based ceramics were applied in many areas such as spark igniters, micro-actuators, sensors, piezo-transformers, transducers and multilayer ceramic capacitors, electro-optical and micro-electromechanical systems applications [4,5].

Recently, the high electrical properties have been reported in binary and ternary systems containing a combination of normal and relaxor ferroelectric materials such as $PbTiO_3$–$Pb(Mg_{1/3}Nb_{2/3})O_3$ (PT–PMN), $Pb(Zr,Ti)O_3$–$Pb(Zn_{1/3}Nb_{2/3})O_3$ (PZT–PZN), $Pb(Zr,Ti)O_3$–$Pb(Ni_{1/3}Nb_{2/3})O_3$ (PZT–PNN) [3,6–9], $PbZrO_3$–$PbTiO_3$–$Pb(Mg_{1/3}Nb_{2/3})O_3$ (PZ–PT–PMN) [10], $PbZrO_3$–$PbTiO_3$–$Pb(Ni_{1/3}Nb_{2/3})O_3$ (PZ–PT–PNN) [7–9] and $Pb(Zn_{1/3}Nb_{2/3})O_3$–$PbZrO_3$

* Corresponding author. Tel.: +66 53 943 376; fax: +66 53 357 512.
E-mail address: rujijanagul@yahoo.com (G. Rujijanagul).

1567-1739/$ - see front matter © 2007 Elsevier B.V. All rights reserved.
doi:10.1016/j.cap.2007.05.002

(PZN–PZ) [4]. The solid solution of lead nickel niobate $Pb(Ni_{1/3}Nb_{2/3})O_3$ (PNN) with $Pb(Zr_{1-x}Ti_x)O_3$ (PZT) is also a relaxor-type ferroelectrics, which has drawn much interest in recent years for its excellent dielectric, especially electrostrictive properties [7–9]. Our recent work found that the maximum relative permittivity ($\varepsilon_{r(max)}$) of MPB compositions in the PNN–PZT binary systems is higher than 30,000 [3]. However, the properties and phase transition of the lead-based ferroelectric materials are strongly influenced by density, composition, phase, and microstructure which in turn depend on the method of preparation. In the present work, the columbite precursor method and conventional mixed oxide method were used in synthesizing the 0.8PZT–0.2PNN ceramics. The columbite precursor method is used as an initial step of preparing columbite precursor ($NiNb_2O_6$) and wolframite ($ZrTiO_4$) precursor followed by a reaction with PbO to form the binary ceramics system whereas the conventional method utilizes a one-step reaction with all of the starting materials. The phase formation, phase transition and electrical properties of the ceramics prepared by both the methods were compared and discussed.

2. Experiment procedure

Ceramics of the binary system 0.8PZT–0.2PNN were prepared via the columbite method and the conventional method. For the columbite method, the columbite structure ($NiNb_2O_6$) and wolframite structure ($ZrTiO_4$) was synthesized first. $NiNb_2O_6$ was formed by reacting NiO and Nb_2O_5 at 1100 °C for 4 h, while $ZrTiO_4$ was prepared by reaction between ZrO_2 and TiO_2 at 1400 °C for 4 h. The precursors and PbO (with 2 mol% excess PbO) were weighed and mixed by ball-milling in a polyethylene bottle together with partially stabilized zirconia media. The mixture was calcined at 950 °C for 4 h in a double crucible configuration with a heating rate of 20 °C/min. After grinding and sieving, 5 wt.% of polyvinyl alcohol binder was added. The calcined powder was cold isostatically pressed into pellets at a pressure of 150 MPa. The pellets were sintered in a sealed alumina crucible at 1250 °C for 2 h. To compensate PbO volatilization, the PbO atmosphere for the sintering was maintained using $PbZrO_3$ as the spacer powder. For the conventional method, oxides of PbO, NiO, ZrO_2, TiO_2 and Nb_2O_5 were mixed in the required stoichiometric ratios to form the composition 0.8PZT–0.2PNN. The mixture was then followed the same processing condition as the columbite method. The density of the sintered samples was measured by Archimedes' method with distilled water as the fluid medium. Perovskite phase formation of sintered pellets was checked by X-ray diffraction (XRD). The microstructures of the sintered samples were examined using a scanning electron microscopy (SEM). For the electrical measurement, the pellets were polished and then electroded by gold sputtering. The relative permittivity (ε_r) at various temperature was measured using a LCR meter in junction with an environmental chamber with a heating rate of 3 °C/min. The ferroelectric polarization versus electric field (P–E) measurements was made using a Sawyer-Tower circuit at 50 Hz. The ceramics were poled for piezoelectric measurement in silicone oil at 80 °C for 30 min at field strength of 2 kV/mm. The d_{33} piezoelectric coefficient was measured using a d_{33} meter, 24 h after poling.

3. Results and discussion

Fig. 1 shows XRD patterns of the 0.8PZT–0.2PNN ceramics prepared by columbite and conventional methods. Perovskite phase was observed for both the methods. XRD patterns for the ceramics over the range $2\theta = 42–48°$ are shown in Fig. 2. There was appearance of multi peaks due to the superposition of the tetragonal and rhombohedral (200) peaks. In general, the single peak of (200) reflection results for the rhombohedral phase, whereas it

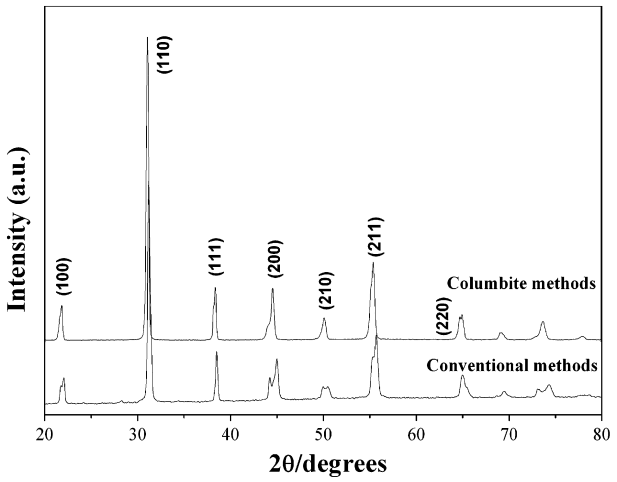

Fig. 1. XRD patterns of 0.8PZT–0.2PNN ceramics prepared by the conventional method and the columbite method.

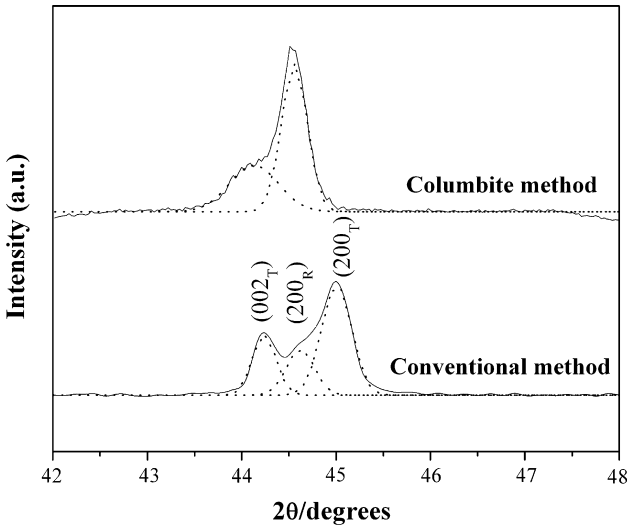

Fig. 2. XRD patterns of the (002) and (200) peaks of 0.8PZT–0.2PNN ceramics prepared by the conventional method and the columbite method.

splits into two peaks for the tetragonal phase. In the present work, the XRD pattern for the columbite prepared sample shows a weak splitting of the (200) peak, while the conventionally prepared sample exhibits a strong splitting of the peak. In order to identify the phase compositions between rhombohedral and tetragonal phase, the (200) peaks can be fitted with Gaussian peaks. For the conventionally prepared sample, it can be well fitted with three Gaussian peaks as seen in Fig. 2. However, it can only be fitted with two peaks for the columbite prepared sample because of the intensive overlap of the (200) tetragonal and (200) rhombohedral plane. The result indicates that the columbite method produced the ceramics with the dominance of the rhombohedral phase (rhombohedral rich) compared with the conventional method. Similar behavior was reported by previous authors in another ferroelectric system [11].

The ceramic density was measured to be 7.49 g/cm^3 and 7.90 g/cm^3 for columbite and conventional methods, respectively. The SEM images of fracture surface for 0.8PZT–0.2PNN ceramics prepared by both the methods are shown in Fig. 3. The porosity levels evident in SEM micrographs of the ceramics were consistent with the density values. In addition, the columbite method produces ceramics with courser grains compared with the conventional method. By using the linear intercept method to the SEM images, the average grain size was determined to be 5.8 and 2.1 μm for the columbite and conventionally prepared samples, respectively. The results suggested that different processing methods develop the ceramics with different density and grain size.

In polar dielectric, in most cases the molecules cannot orient themselves in the low-temperature region. When the temperature rises, the orientation of dipoles facilitates, and this increases the permittivity. Characteristic sets of curves are obtained if the dependence of the permittivity of strong polarized dielectrics is plotted versus two variable factors – temperature and frequency. The variations of the relative permittivity of the material under investigation were measured as a function of temperature between 1 kHz and 100 kHz. From Fig. 4, the temperature dependences of dielectric constant depict a typical relaxor behavior with strong dispersion of the dielectric peak at $T < T_m$ (T_m, the temperature of permittivity maximum) for both methods. The broad dielectric maxima shifting towards higher temperature with increasing frequency signify the

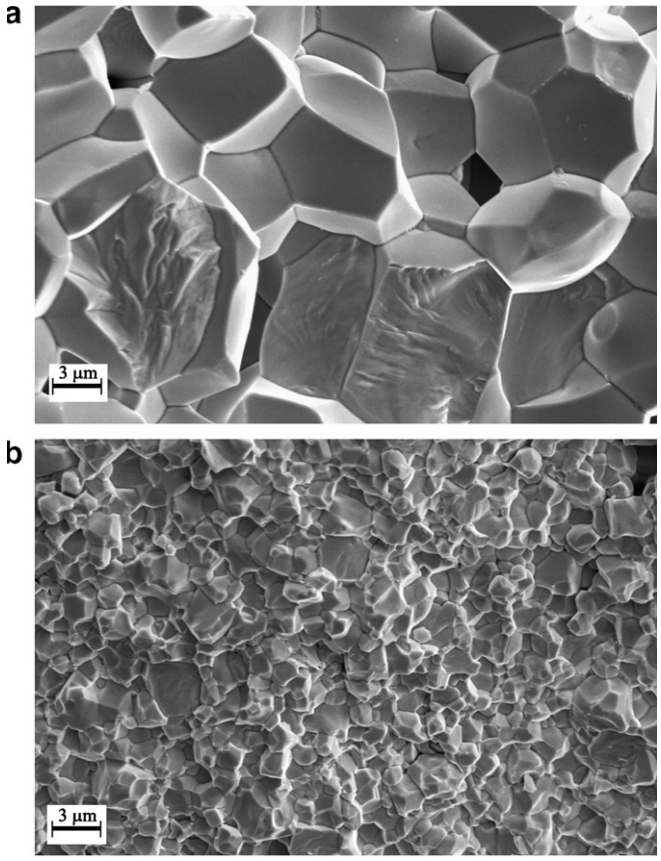

Fig. 3. Fracture surface of 0.8PZT–0.2PNN ceramics prepared by (a) columbite method and (b) conventional method.

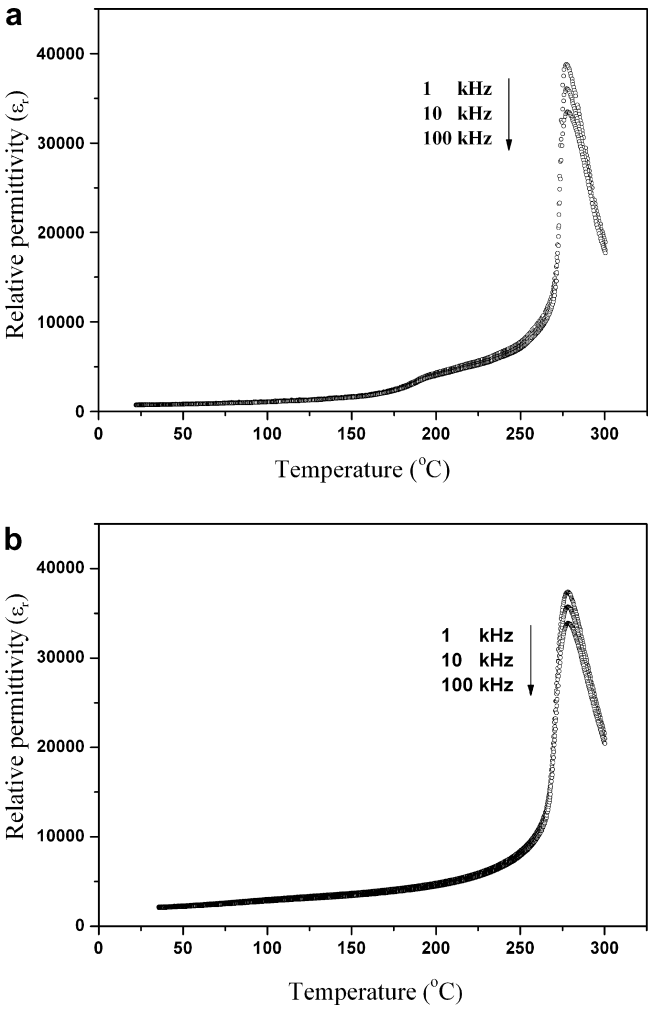

Fig. 4. Temperature dependence on the relative permittivity of 0.8PZT–0.2PNN at frequencies between 1 kHz and 100 kHz: (a) columbite method; (b) conventional method.

relaxor-like type behavior of the ceramics. Furthermore, the columbite prepared sample shows stronger frequency dependence compared with the conventional prepared sample. However, the frequency dispersion in the 0.8PZT–0.2PNN ceramics prepared by both the methods is not as strong as that in the pure relaxor PZN. Fig. 5 shows a comparison dielectric result (measured at 10 kHz) between the conventional and columbite prepared sample. The temperature at which the permittivity is maximum T_m and the relative permittivity (measured at 10 kHz) for both at room temperature and at T_m is listed in Table 1. The columbite prepared sample shows a sharp dielectric maximum at the ferroelectric transition temperature (T_m) of 277 °C with maximum permittivity value of 36,000 and the conventionally prepared sample exhibits a maximum permittivity value of 35,700 at $T_m \sim 278$ °C. Although the columbite method helps to improve the dielectric permittivity, the porosity of the samples was also found to influence on this value. Therefore, the ceramic prepared via columbite method exhibits a slightly higher relative permittivity at T_m than that of ceramics synthesized by the conventional method.

The ε_r versus T curves shown in Fig. 4 are also indicative of thermally induced phase transitions. The permittivity shows a shoulder at the rhombohedral to tetragonal phase transition temperature ($T_{Rho-Tetra}$) ~ 195 °C for the columbite prepared sample as seen in the Fig. 5. However, for the conventional method, there was observed only one peak present at the tetragonal to cubic phase transition $T_m \sim 278$ °C. Similar transition (rhombohedral to tetragonal transition) has been reported by previous authors in other systems [3,12]. The results for the rhombohedral to tetragonal transition can be related to the XRD results, i.e. rhombohedral rich composition was observed in ceramic prepared by columbite method.

In relaxor ferroelectric materials, the value of relative permittivity above T_m does not follow the Curie–Weiss law. A number of materials show behavior intermediate between proper ferroelectric and relaxor. A simple quadratic law can be used to describe a second order relaxor ferroelectric. This arises from the fact that the total number of relaxors contributing to the permittivity response in the vicinity of the permittivity peak is temperature dependent. The diffusiveness parameter (δ_γ) of the transition was determined from the equation [13,14]:

$$\frac{\varepsilon_{r(max)}}{\varepsilon_r} = \exp\left(\frac{(T - T_m)^2}{2\delta_\gamma^2}\right) \quad (1)$$

where $\varepsilon_{r(max)}$ is maximum value of the relative permittivity at $T = T_m$ and ε_r is the dielectric constant of sample. The value of the diffuseness parameter can be calculated from the slope of $\ln(\varepsilon_{r(max)}/\varepsilon_r)$ versus $(T - T_m)^2$ curve. This value is valid for the range of $\varepsilon_{r(max)}/\varepsilon_r < 1.5$, as clarified by Pilgrim et al. [13]. The graphs of $\ln(\varepsilon_{r(max)}/\varepsilon_r)$ versus $(T - T_m)^2$ is shown in Fig. 6. The values of parameter δ_γ are listed in Table 1. The parameter δ_γ is calculated to be 14.6 and 16.1 in ceramics prepared with columbite method and conventional method, respectively. A significant increase in δ_γ for the conventionally prepared sample indicates an increased diffusiveness in the phase transition. This may be due to the homogeneity at the atomic scale of the columbite

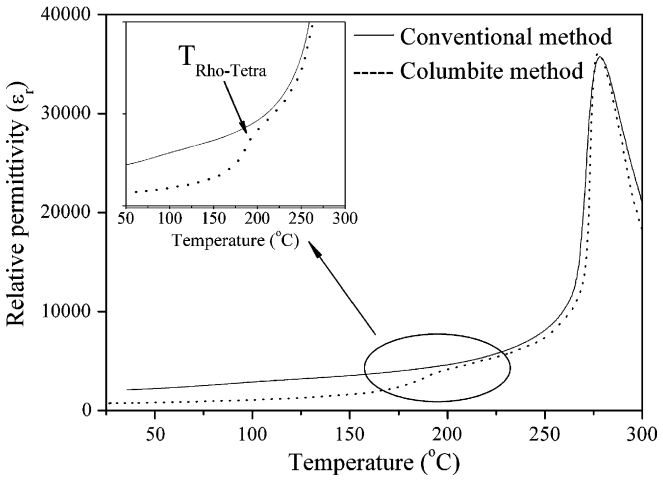

Fig. 5. Temperature dependence on the relative permittivity of 0.8PZT–0.2PNN ceramics prepared by the conventional method and the columbite method measured at 10 kHz.

Table 1
Comparisons of dielectric properties measured at 10 kHz of 0.8PZT–0.2PNN ceramics prepared by the conventional method and the columbite method

Method of preparation	ε_r at 25 °C	$\tan\delta$ at 25 °C	T_m (°C)	$\varepsilon_{r(max)}$	$\tan\delta$ at T_m	δ_γ (°C)
Columbite method	825	0.011	277	36,000	0.047	14.6
Conventional method	2100	0.014	278	35,700	0.030	16.1

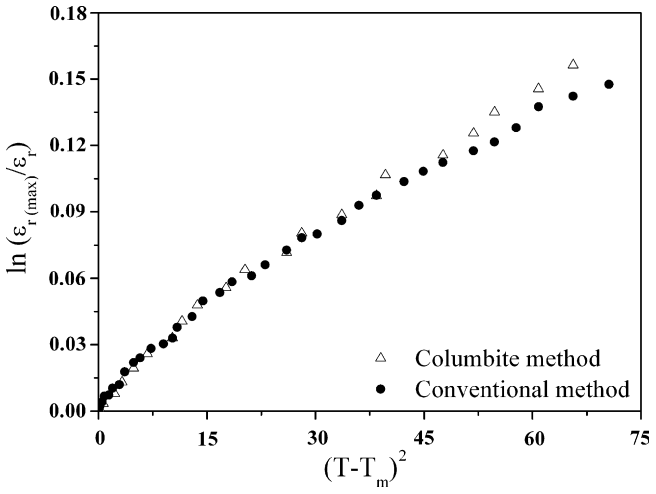

Fig. 6. The $\ln(\varepsilon_{r(max)}/\varepsilon_r)$ versus $(T - T_m)^2$ for 0.8PZT–0.2PNN ceramics prepared by the conventional method and the columbite method.

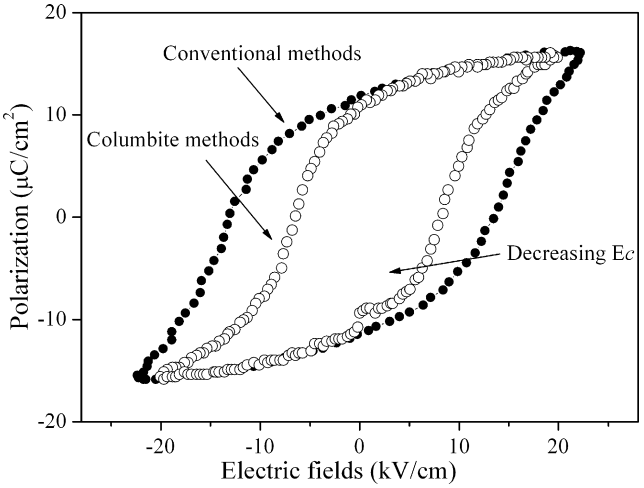

Fig. 7. P–E hysteresis of 0.8PZT–0.2PNN ceramics prepared by the conventional method and the columbite method.

prepared sample which is much higher than that in the ceramics prepared by conventional method.

The result of polarization–field (P–E) measurement (at 50 Hz) for ceramics prepared from both the methods is shown in Fig. 7. The polarization loop of both samples are well developed showing a large remanent polarization at zero field. The hysteresis loops have a typical "square" form stipulated by switching of a domain structure in an electrical field, which is typical of a phase that contains long-range cooperation between dipoles. That is characteristic of a ferroelectric micro-domain state. From the fully saturated loops, the remanent polarization P_r and coercive field E_c were determined. The values of P_r and E_c for conventional method are 10.1 μC/cm^2 and 13.3 kV/cm, respectively, whereas for columbite methods the remanent polarization P_r and coercive field E_c are 10.9 μC/cm^2 and 7.2 kV/cm, respectively. It can be noted that P_r for the columbite method is not too much higher than the conventional method, which may be due to the porosity effect. However, the higher P_r and lower E_c can be related to the more rhombohedral phase in the columbite prepared sample [15]. This trend is agreed with the results from the previous works in PMN–PZ–PT and PZT ceramics [16,17].

In order to study the piezoelectric property of the samples, the d_{33} piezoelectric coefficient was measured at the same condition. The d_{33} values were found to be 282 and 202 pC/N for the ceramics prepared by conventional and columbite method, receptively. The d_{33} value for the conventional method is relatively high compared to those reported in the literature for the same system [18]. However, d_{33} value for the columbite sample was lower than the conventional method. The lower d_{33} value is likely due to the higher porosity of the columbite prepared sample. This effect also made the ceramics difficult to pole.

4. Conclusions

The properties of 0.8PZT–0.2PNN ceramics prepared by the conventional method and the columbite methods were investigated. Phase transition behavior, dielectric, and ferroelectric properties were found to depend on the phase composition of the samples with association with the methods of preparation. Although a slightly higher dielectric constant was observed in the columbite prepared sample, the better piezoelectric property was found for the conventionally prepared sample. These results were attributed to the porosity effect.

Acknowledgements

This work was supported by The Thailand Research Fund (TRF), Faculty of Science Chiang Mai University, King Mongkut's Institute of Technology Ladkrabang (KMITL), and Commission on Higher Education (CHE) Thailand. The authors would like to thank Prof. Dr. Tawee Tunkasiri for his help in many facilities.

References

[1] G.A. Smolenskii, A.L. Agranovskaya, Sov. Phys. Tech. Phys. 2 (1958) 1380.
[2] C.A. Randall, A.S. Bhalla, Jpn. J. Appl. Phys. 29 (1990) 327.
[3] N. Vittayakorn, G. Rujijanagul, X. Tan, M.A. Marquardt, D.P. Cann, J. Appl. Phys. 96 (12) (2004) 5103.
[4] Y. Xu, Ferroelectric Materials and Their Application, Elsevier Science Publishers B.V., 1991.
[5] K. Uchino, Ferroelectrics 151 (1994) 321.
[6] K. Uchino, Solid State Ionics 108 (1998) 43.
[7] N. Vittayakorn, C. Puchmark, G. Rujijanagul, X. Tan, D.P. Cann, Curr. Appl. Phys. 6 (2006) 303.
[8] N. Vittayakorn, G. Rujijanagul, X. Tan, H. He, M.A. Marquardt, D.P. Cann, J. Electroceram 16 (2006) 141–149.
[9] N. Vittayakorn, G. Rujijanagul, T. Tunkasiri, X. Tan, D.P. Cann, Mat. Sci. Eng. B 108 (2004) 258.
[10] R. Yimnirun, S. Ananta, P. Laoratanakul, J. Eur. Ceram. Soc. 25 (2005) 3235.
[11] H. Fan, H.E. Kim, J. Am. Ceram. Soc. 84 (3) (2001) 636.
[12] M.-S. Yoon, H.M. Jang, J. Appl. Phys. 77 (1995) 3991.
[13] S.M. Pilgrim, A.E. Sutherland, S.R. Winzer, J. Am. Ceram. Soc. 73 (10) (1990) 3122.
[14] N. Vittayakorn, S. Uttiya, G. Rujijanagul, D.P. Cann, J. Phys. D: Appl. Phys. 38 (2005) 2942–2946.
[15] K.H. Yoona, H.R. Lee, J. Appl. Phys. 89 (7) (2001) 3915.
[16] W.Z. Zhu, A. Kholkin, P.Q. Mantas, J.L. Baptista, J. Mater. Sci. 36 (2001) 3447.
[17] T. Yamamoto, H. Moriwake, J. Korean Phys. Soc. 32 (1998) S1301.
[18] X. Zhu, Z. Meng, J. Mater. Sci. 31 (1996) 2171.

Available online at www.sciencedirect.com
ScienceDirect
Current Applied Physics 8 (2008) 128–133
Current Applied Physics
An official journal of the KPS
www.elsevier.com/locate/cap
www.kps.or.kr

Development of perovskite and phase transition in lead cobalt niobate modified lead zirconate titanate system

Naratip Vittayakorn [a,*], Supamas Wirunchit [a], Sakda Traisak [a], Rattikorn Yimnirun [b], Gobwut Rujijanagul [b]

[a] *Materials Science Research Unit, Department of Chemistry, Faculty of Science, King Mongkut's Institute of Technology Ladkrabang, Bangkok 10520, Thailand*

[b] *Department of Physics, Faculty of Science, Chiang Mai University, Chiang Mai 50200, Thailand*

Received 19 December 2006; received in revised form 28 May 2007; accepted 15 June 2007
Available online 29 June 2007

Abstract

Ferroelectric lead zirconate titanate–lead cobalt niobate ceramics with the formula $(1-x)Pb(Zr_{1/2}Ti_{1/2})O_3$–$xPb(Co_{1/3}Nb_{2/3})O_3$ where $x = 0.0$–0.5 were fabricated using a high temperature solid-state reaction method. The formation process, the structure and homogeneity of the obtained powders have been investigated by X-ray diffraction method as well as the simultaneous thermal analysis of both differential thermal analysis (DTA) and thermogravimetry analysis (TGA). It was observed that for the binary system $(1-x)Pb(Zr_{1/2}Ti_{1/2})O_3$–$xPb(Co_{1/3}Nb_{2/3})O_3$, the change in the calcination temperature is approximately linear with respect to the PCoN content in the range $x = 0.0$–0.5. In addition, X-ray diffraction indicated a phase transformation from a tetragonal to a pseudo-cubic phase when the fraction of PCoN was increased. The dielectric permittivity is remarkably increased by increasing PCoN concentration. The maximum value of remnant polarization P_r (25.3 $\mu C/cm^2$) was obtained for the 0.5PZT–0.5PCoN ceramic.

PACS: 77.22.−d; 77.80.Bh; 77.84.Dy; 61.10.Nz; 77.80.Dj

Keywords: Ferroelectric; Relaxor ferroelectric; Perovskite

1. Introduction

Since the late 1960s, lead titanate:lead zirconate ceramic (generally known as $Pb(Zr_{1-x}Ti_x)O_3$ or PZT), near the tetragonal–rhombohedral morphotropic phase boundary has been considered an important material for a wide range of piezoelectric, pyroelectric and ferroelectric device applications such as transducers, computer memory and display and pyroelectric sensors [1,2]. Most commercial PZT ceramics are thus designed in the vicinity of the morphotropic phase boundary (MPB) with various doping in order to achieve optimum properties [1,2]. Recently, many piezoelectric ceramic materials have been developed from binary systems containing a combination of relaxor and normal ferroelectric materials [3] which yield high dielectric permittivities {e.g. $Pb(Zn_{1/3}Nb_{2/3})O_3$–$PbTiO_3$ (PZN–PT) [4,5], $Pb(Zr_{1/2}Ti_{1/2})O_3$–$Pb(Ni_{1/3}Nb_{2/3})O_3$ (PZT–PNN) [6]}, excellent piezoelectric coefficients {e.g. $Pb(Zn_{1/3}Nb_{2/3})O_3$–$PbTiO_3$ (PZN–PT) [4,5], $Pb(Zr_{1/2}Ti_{1/2})O_3$–$Pb(Zn_{1/3}Nb_{2/3})O_3$ (PZN–PZT) [7], $Pb(Sc_{1/3}Nb_{2/3})O_3$–$PbTiO_3$ (PSN–PT) [8,9]}, and high pyroelectric coefficients {e.g. $Pb(Ni_{1/3}Nb_{2/3})O_3$–$PbTiO_3$–$PbZrO_3$(PNN–PT–PZ) [10]}.

Lead cobalt niobate ($Pb(Co_{1/3}Nb_{2/3})O_3$, PCoN) is a typical relaxor ferroelectric characterized by a high dielectric constant, a broad diffuse phase transition near −70 °C and low firing temperature [11]. Though the paraelectric–ferroelectric transition temperature of PCoN is below room temperature, it can be easily shifted upward with the

* Corresponding author. Tel.: +66 89 700 2136; fax: +66 2 326 4415.
E-mail address: naratipcmu@yahoo.com (N. Vittayakorn).

1567-1739/$ - see front matter © 2007 Elsevier B.V. All rights reserved.
doi:10.1016/j.cap.2007.06.002

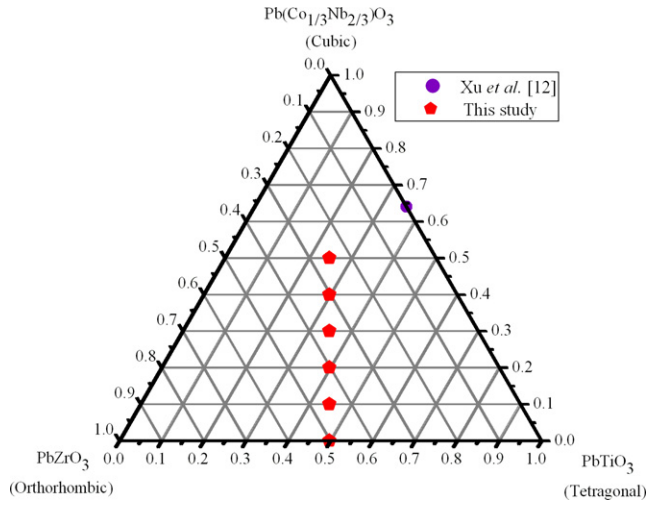

Fig. 1. Compositions studied in the $PbTiO_3$–$PbZrO_3$–$Pb(Co_{1/3}Nb_{2/3})O_3$ ternary system.

addition of $PbTiO_3$ (PT), which is a normal ferroelectric compound with a phase transition at 490 °C. So the PCoN-based relaxors are one of the most attractive materials for multilayer ceramic capacitors and electrostrictive actuators [2].

Since PCoN is a relaxor ferroelectrics with a broad dielectric peak near $T_c \approx -70$ °C and PZT (Zr/Ti = 50/50) is a normal ferroelectric with a sharp maximum permittivity at $T_c \sim 390$ °C, the curie temperature in PZT–PCoN system can be engineered over a wide range of temperature by controlling the amount of PCoN in the system. However, the PZT–PCoN ceramics have not been obtained as yet. Fig. 1 schematically shows the pseudo-ternary composition range which was studied in this work compared with other studies [2]. In order to get more information about combination of relaxor and normal ferroelectric materials and to recognize the properties of PZTCoN ceramics, this paper attempted to carry out the synthesis of the quasi-binary solid solution $(1-x)Pb(Zr_{0.5}Ti_{0.5})O_3$–$xPb(Co_{1/3}Nb_{2/3})O_3$, with $x = 0.0$–0.5 using a solid-sate reaction method and to report some properties of obtained ceramics.

2. Experimental

Ceramics of $(1-x)Pb(Zr_{0.5}Ti_{0.5})O_3$–$xPb(Co_{1/3}Nb_{2/3})O_3$(PZT–PCoN) with $x = 0$–0.5 were synthesized using the solid-state reaction method. The CoO (99.9%), Nb_2O_5 (99.9%), PbO (Fluka, >99% purity) TiO_2 (99.8%) and ZrO_2 (99%) were mixed and milled in ethyl alcohol for 18 h using a ball-milling. After drying at 120 °C for 2 h, the reaction of the uncalcined powders taking place during heat treatment was investigated by differential thermal analysis (DTA; Shimadzu) and thermogravimetry analysis (TGA; Shimadzu), using a heating rate of 10 °C/min in air from room temperature up to 1400 °C. Based on the TG–DTA results, the mixture was calcined at various temperatures ranging from 650 to 900 °C, dwell times 4 h and heating/cooling rates ranging 20 °C/min, in closed alumina crucible, in order to investigate the perovskite phase formation. The calcined powders, with polyvinyl alcohol (PVA) added as binder, were pressed into pellets of 15 mm diameter and ~2 mm thickness, which were then sintered at 1100–1200 °C in Pb-atmosphere for 4 h in a closed alumina crucible. X-ray diffraction (XRD; Philips PW 1729 diffractometer) using Cu K_α radiation was used to determine the phases formed and optimum firing temperatures for the formation of desired phase. For measuring the dielectric and ferroelectric characteristics, the specimens were polished to 1 mm thickness. After ultrasonic cleaning in ethanol bath, silver-paste was coated on the polished samples on both sides by the screen printing method, and then subsequently, fired at 650 °C for 30 min. For the dielectric properties measurement, capacitance was measured at 1 kHz using an automated measurement system consisted of an LCR meter (HP-4284, Hewlett–Packard Inc.). The dielectric constant is then calculated from $\varepsilon_r = Cd/\varepsilon_0 A$, where C is the capacitance of the sample, d and A are the thickness and the area of the electrode, respectively, and ε_0 is the dielectric permittivity of vacuum (8.854×10^{-12} F/m). The ferroelectric hysteresis loop parameters were measured with aid of a home-built Sawyer–Tower circuit.

3. Results and discussion

The TG–DTA simultaneous analysis of a powder mixed in the stoichiometric proportions of PZT–PCoN is illustrated in Fig. 2. In the temperature range from room temperature to ~350 °C, the sample shows both exothermic and endothermic peaks in the DTA curve, in consistent with a slight drop in weight loss at the same temperature range. These observations can be attributed to the decomposition of the organic species from the milling process [12,13]. The different temperature, intensities, and shapes of the thermal peaks probably are related to the different natures of the organic species and consequently, caused

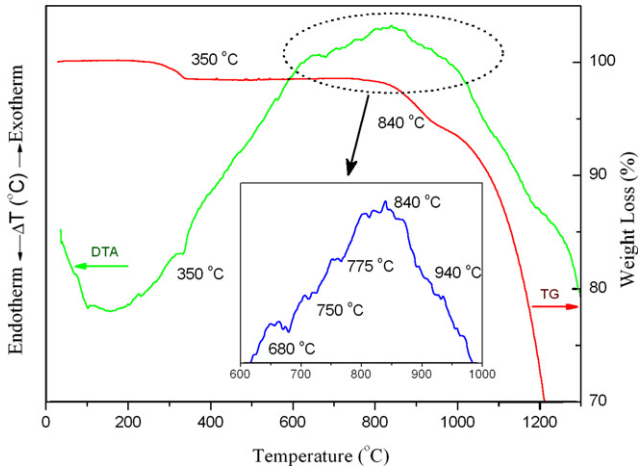

Fig. 2. DTA–TG curves for the mixture of PZT–PCoN powder.

by the removal of species differently bounded in the network [13]. In the temperature range 650–900 °C, both exothermic and endothermic peaks are observed in the DTA curve. The enlarged zone of this DTA curve shows that the endothermic peak at ~750 °C should be correlated to the phase transition of perovskite structure, because no weight loss could be found in the TG curve and that is also in accordance to literature data [14,15]. The last endothermic peak centered at ~840 °C may be caused by the decomposition of lead oxide. As a result, crystallization of PZT–PCoN powders is established above ~750 °C. Further increase in temperature or heating time will promote crystallization of perovskite phase powders. These data were used to define the range of temperatures (650–950 °C) for XRD investigation. To study the phase development with increasing calcination temperature, all compositions were calcined at various temperatures for 4 h in air with constant heating/cooling rates of 20 °C/min, followed by phase analysis using XRD technique.

XRD patterns of the calcined 0.7PZT–0.3PCoN powders at different calcination temperatures are illustrated Fig. 3. The XRD results show that the pyrochlore phase $Pb_xNb_yO_z$ pyrochlore phases was dominant at calcination temperatures below 700 °C. In the work by Chen et al. [12] it was reported that in the lead–niobium pyrochlore system the cubic $Pb_3Nb_4O_{13}$, pyrochlore phase (ICDD No. 25–443) forms first around 580 °C. At higher temperatures, it transforms to $Pb_2Nb_2O_7$, (ICDD No. 40–828) and finally to $Pb_3Nb_2O_8$, (ICDD No. 30–712) with increased calcination temperatures. At 700 °C, the pyrochlore phase began to decrease and disappeared completely at 750 °C. The yield of the perovskite phase increased significantly until at 750 °C, a single-phase of perovskite phase was formed. The studies also reflect the growth of crystallinity in the powders with the increasing heat-treatment temperatures. The results of the X-ray diffraction measurement support the DTA observation (Fig. 2) that the perovskite phase is formed at approximately 750 °C. The relationship between the relative content of perovskite phase and the calcination temperature is illustrated in Fig. 4. The relative content of perovskite phase is calculated based on the value of $(I_{Pe(110)}/(I_{Pe(110)} + I_{Py(222)}))$, where $I_{Pe(110)}$ and $I_{Py(222)}$ indicate the intensity of the (1 1 0) diffraction peak of perovskite phase and the intensity of the (2 2 2) diffraction peak of the pyrochlore phase, respectively. Based on the XRD data obtained here together with the % phase perovskite, it may be conclude that the change in the calcination temperature is approximately linear with respect to the PCoN content in the range $x = 0.0$–0.5. With an increase in x, the calcination temperature shifts up to high temperatures. The XRD patterns of $(1-x)$PZT–xPCoN ceramics with various x values are shown in Fig. 5. The patterns show single-phase perovskite-structured ceramics with $x \leqslant 0.4$. Evidence for the pyrochlore or other second phases was not detected in the patterns. Pyrochlore peaks, identified with "*" in Fig. 5, were found in the samples with $x = 0.5$. These results indicated that the presence of PCoN in the solid solution decreases the structural stability of PZT perovskite phase by its tolerance factor and electronegativity [16].

The $PbZrO_3$–$PbTiO_3$ phase diagram predicts that at room temperature $Pb(Zr_{1/2}Ti_{1/2})O_3$ falls within the tetragonal phase field near the MPB. The crystal symmetry for pure PCoN is cubic at room temperature. Below $T_{max} \approx -70$ °C, the symmetry changes to rhombohedral. Therefore, with increasing x the crystal symmetry should change due to the effects of the increased PCoN fraction and the decrease in T_C. It is well know that in the pseudo-cubic phase, the {2 0 0} profile will show a single narrow peak because all the planes of {2 0 0} share the same lattice parameters, while in the tetragonal phase, the {2 0 0} profile should be split into two peaks with the intensity height of the former being half of the latter because the

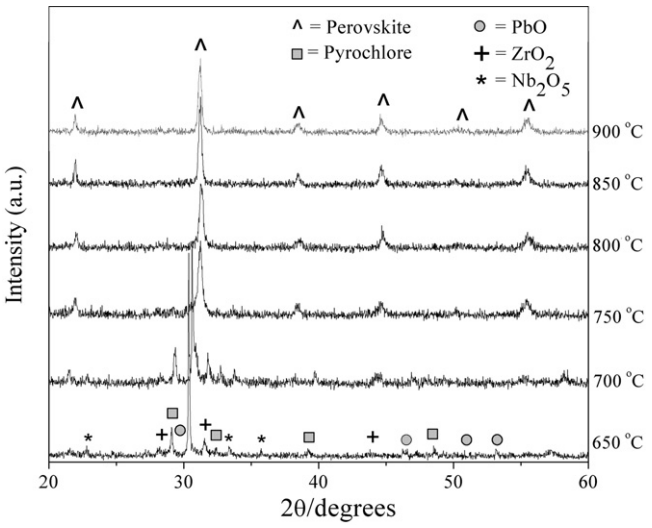

Fig. 3. XRD patterns of 0.7PZT–0.3PCoN powder calcined at various temperature for 4 h.

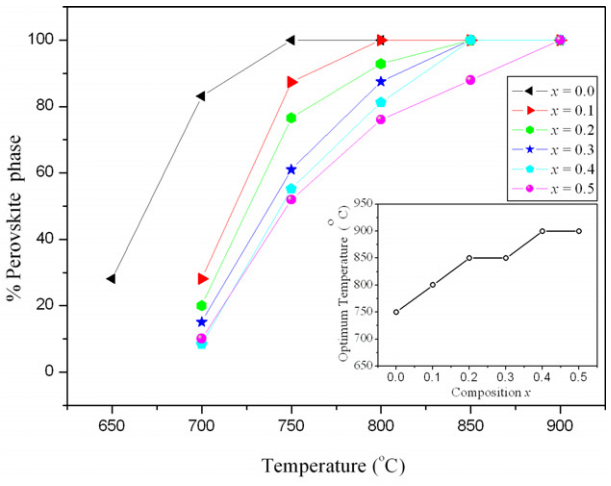

Fig. 4. Percentage of perovskite phase as a function of calcinations temperature for $(1 - x)$PZT–xPCoN powder.

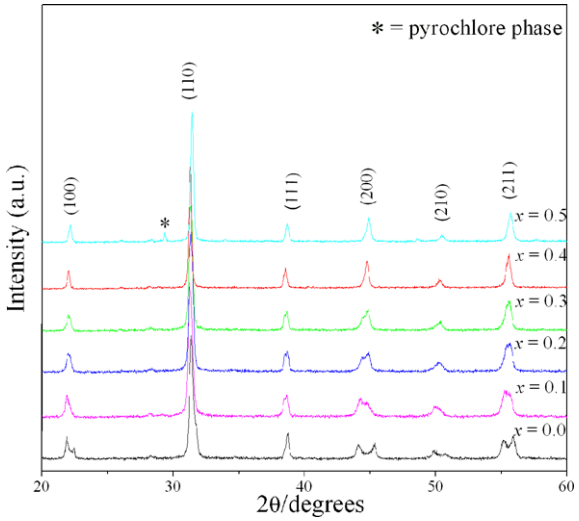

Fig. 5. XRD patterns of $(1-x)$PZT–xPCoN ceramics.

lattice parameters of (200) and (020) are the same but are slightly different from those of (002).

Based on the careful XRD study of {200} reflections in Fig. 6, we can find that a phase transformation from the tetragonal structure to the pseudo-cubic structure occurs with increasing PCoN content. The ceramics exist as tetragonal phase which is indicated by the splitting of $(002)_T$ and $(200)_T$ peaks in the 2θ range from 43.5° to 46.5° at $x = 0.10$. As PCoN content increases from $x = 0.1$ to 0.3, the ceramics coexist as tetragonal and pseudo-cubic phase revealed by the coexistence of $(002)_T$ and $(200)_R$ peaks in the 2θ range from 43.5° to 45.5°. To a first approximation, it could be said that the composition with $x = 0.1$–0.2 is close to the morphotropic phase boundary (MPB) of the $Pb(Zr_{0.50}Ti_{0.50})O_3$–$Pb(Co_{1/3}Nb_{2/3})O_3$ system, where the structure of the PZT–PCoN compositions is gradually changing from tetragonal to pseudo-cubic. Electrical data described later further supports this assumption.

The ceramics with $x = 0.50$ exist as pseudo-cubic phase revealed by the single $(200)_R$ peak. It is interesting to note that the influence of the addition of $Pb(Co_{1/3}Nb_{2/3})O_3$ on the phase transition of the $Pb(Zr_{1/2}Ti_{1/2})O_3$ system is similar to that of $Pb(Zr_{1/2}Ti_{1/2})O_3$–$Pb(Ni_{1/3}Nb_{2/3})O_3$, $Pb(Zr_{1/2}Ti_{1/2})O_3$–$Pb(Mg_{1/3}Nb_{2/3})O_3$ and $Pb(Zr_{1/2}Ti_{1/2})O_3$–$Pb(Zn_{1/3}Nb_{2/3})O_3$ systems [6,17–19].

The dielectric properties of $(1-x)$PZT–xPCoN, $x = 0.0$–0.5 are illustrated in Fig. 7. With increasing concentration of PCoN, the dielectric constant tends to increase. The effect of increasing the dielectric constant at room temperature with increasing PCoN content is interpreted to be due to the possibility of the decrease of the transition temperature to near room temperature. Because of when PCoN is added into PZT, the transition temperature of the PZT–PCoN ceramics are shifted towards the room temperature; hence the dielectric properties measured at room temperature are increased. Other authors have reported a similar behavior [6,20]. Fig. 8 shows the saturated loops of 0.9PZT–0.1PCoN samples with difference electric fields strengths. It is clearly evident that the shape of hysteresis various greatly with the electric fields strength. At 5 kV/cm electric fields strength, a near-linear relationship of P–E is observed. This result is due to the fact that the electric field is not large enough to switch any domains. At 10 kV/cm electric fields, the polarization nonlinearity is developed in both regions of the positive and negative fields. These results clearly demonstrate that the electric field strength of 10 kV/cm is of enough energy to constrain realignment of some domains in the direction of the applied fields. No evidence of pinning effect or asymmetric loop was detected in all electric fields strength. At 25 kV/cm electric field strength, the loop reveals fully developed symmetric hysteresis loop. This shows that the electric fields strength of 25 kV/cm has of enough energy to constrain realignment of all domains in the direction of the electric fields.

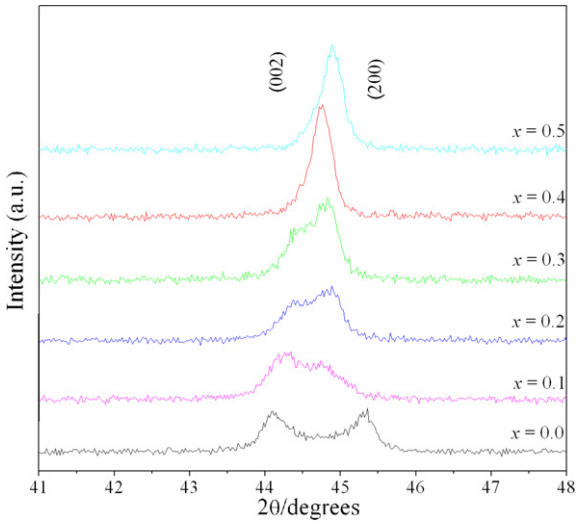

Fig. 6. XRD pattern of the (200) peak of $(1-x)$PZT–xPCoN, $x = 0.0$–0.1 ceramics.

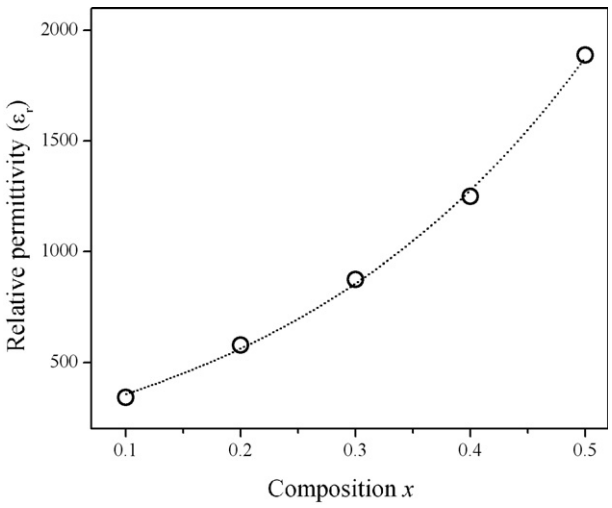

Fig. 7. Relative permittivity of $(1-x)$PZT–xPCoN as a function of compositions.

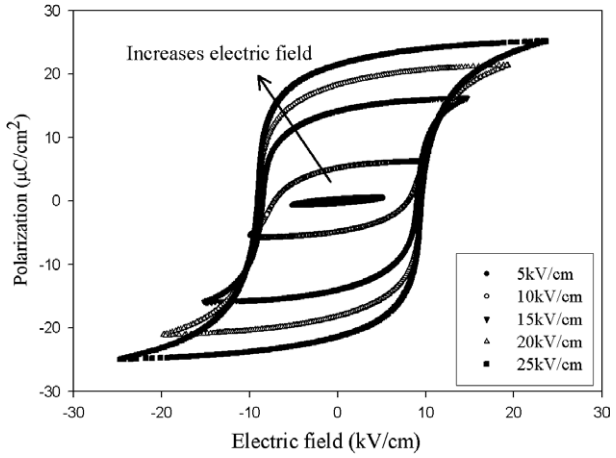

Fig. 8. Polarization of $(1-x)$PZT–xPCoN ceramics with $x = 0.1$ as a function of electric fields.

Fig. 9 illustrates the P–E curves of the samples with $x = 0.0$, 0.1 and 0.5 measured at 25 kV/cm. All compositions show symmetry in shape and reveal rectangular hysteresis loops. From the fully saturated loops, the remanent polarization P_r and coercive field E_c were determined. The values of P_r and E_c for composition $x = 0.1$ are 21.4 μC/cm^2 and 9 kV/cm, respectively, whereas for composition $x = 0.0$ the remanent polarization P_r is 15.2 μC/cm^2. At the composition $0.0 \leqslant x \leqslant 0.5$, the hysteresis loop has a typical "square" form stipulated by switching of a domain structure in an electrical field, which is typical of a phase that contains long-range cooperation between dipoles. That is characteristic of a ferroelectric micro-domain state. Room temperature values of P_r are found to be ~15.2, 21.4 and 25.3 μC/cm^2 for composition $x = 0.0$, 0.1 and 0.5 samples, respectively. The results on other compositions are also listed Table 1.

It is seen that the samples with compositions $x = 0.1$ and 0.5 exhibit the highest saturation and remnant polarization among all the ceramics studied. As indicated by the above

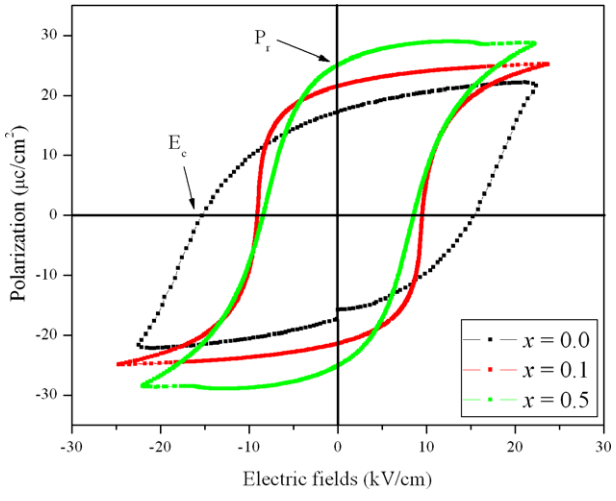

Fig. 9. Hysteresis loops of the $(1-x)$PZT–xPCoN ceramics with $x = 0.0$, 0.1 and 0.5 measured at 25 kV/cm.

Table 1
Polarization hysteresis data as a function of x in the $(1-x)$PZT–xPCoN system

Composition	P_s (μC/cm^2)	P_r (μC/cm^2)	E_c (kV/cm)
$x = 0.0$	19.3	15.2	16.7
$x = 0.1$	25.0	21.4	9.0
$x = 0.2$	10.1	9.5	9.7
$x = 0.3$	12.5	7.6	8.4
$x = 0.4$	13.9	8.6	9.8
$x = 0.5$	28.7	25.3	9.3

XRD, the composition with $x = 0.1$ contains both tetragonal and pseudo-cubic phases, so it should favor a strong ferroelectric effect due to the increased ease of reorientation during poling by transformation of a number of 180° domains into 90° ones. From the present results, it also can be revealed that the MPB coexisting in the tetragonal and pseudo-cubic phases in the present system is a broad composition region of $x \sim 0.1$, which exhibits high ferroelectric properties around the center of the MPB. Recent literature reviews [18,21] show that there are 2 MPBs in the PZT–PZN system; first, the separated tetragonal phase with rhombohedra phase at the composition 0.8PZT–0.2PZN and the second MPB showing transformation relaxor pseudo-cubic ferroelectric to normal pseudo-cubic ferroelectric at the composition 0.5PZT–0.5PZN [7]. It is interesting to note that the composition $x = 0.5$ in PZT–PCoN system may be attributed to the transition from normal ferroelectric to relaxor ferroelectric which is similar to the PZT–PZN and PZT–PNN system [6,7,21].

4. Conclusions

The effect of PCoN modification on the phase formation and transition mechanism of perovskite PZT–PCoN ceramics has been investigated for various chemical compositions. X-ray diffraction has indicated that except at $x = 0.5$, complete solid solutions occur across the entire compositional range of the $(1-x)Pb(Zr_{0.5}Ti_{0.5})O_3$–$xPb(Co_{1/3}Nb_{2/3})O_3$ system. PZT ceramic was identified by XRD as a single-phase material with a perovskite structure having tetragonal symmetry, while the mixed compositions showed a gradual change from tetragonal to pseudo-cubic symmetry, with a possible morphotropic phase boundary (MPB) between the two phases near the 0.9PZT–0.1PCoN composition. Ferroelectric and dielectric properties of the PZT–PCoN ceramics were investigated. The maximum value of remnant polarization P_r (25.3 μC/cm^2) was obtained for the 0.5PZT–0.5PCoN ceramic. Most importantly, this study showed that the addition of PCoN could improve the ferroelectric behavior in PZT ceramics.

Acknowledgements

This work was supported by the Thailand Research Fund (TRF), the Commission on Higher Education (CHE), National Research Council of Thailand (NRCT),

Thailand Graduate Institute of Science and Technology (TGIST) and King Mongkut's Institute of Technology Ladkrabang (KMITL).

References

[1] K. Uchino, Ferroelectric Devices, Marcel Dekker, Inc., New York, 2000.
[2] Y. Xu, Ferroelectric Materials and Their Application, Elsevier Science Publishers B.V., 1991.
[3] S.-E. Park, T.R. Shrout, IEEE Tr. UFFC. 44 (1997) 1140.
[4] J. Kuwata, K. Uchino, S. Nomura, Ferroelectrics 37 (1981) 579.
[5] M.L. Mulvihill, L.E. Cross, W. Cao, K. Uchino, J. Am. Ceram. Soc. 80 (1997) 1462.
[6] N. Vittayakorn, G. Rujijanagul, X. Tan, M.A. Marquardt, D.P. Cann, J. Appl. Phys. 96 (2004) 5103.
[7] H. Fan, H.-E. Kim, J. Mater. Res. 17 (2002) 180.
[8] O. Furukawn, Y. Yamashita, M. Harata, T. Takahashi, K. Inagai, Jpn. J. Appl. Phys. 24 (1985) 96.
[9] V.J. Tennery, K.W. Hang, R.E. Novak, J. Am.Ceram. Soc. 51 (1968) 671.
[10] D. Luff, R. Lane, K.R. Brown, H.J. Marshallsay, Trans. J. Br. Ceram. Soc. 73 (1974) 251.
[11] G.A. Smolenskii, A.L. Agranovskaya, Sov. Phys.-Tech. Phys. (1958) 1380.
[12] A. Ngamjarurojana, O. Khamman, R. Yimnirun, S. Ananta, Mater. Lett. 60 (2006) 2867.
[13] N. Vittayakorn, S. Wirunchit, Smart Mater. Struct. 16 (2007) 851.
[14] R. Wongmaneerung, R. Yimnirun, S. Ananta, Mater. Lett. 60 (2006) 2666.
[15] R. Wongmaneerung, T. Sarakonsri, R. Yimnirun, S. Ananta, Mater. Sci. Eng. B 130 (2006) 246.
[16] T.R. Shrout, A. Halliyal, Am. Ceram. Soc. Bull. 66 (1987) 704.
[17] N. Vittayakorn, C. Puchmark, G. Rujijanagul, X. Tan, D.P. Cann, Curr. Appl. Phys. 6 (2006) 303.
[18] N. Vittayakorn, G. Rujijanagul, X. Tan, H. He, M.A. Marquardt, D.P. Cann, J. Electroceram. 16 (2006) 141.
[19] S. Wongsaenmai, Y. Laosiritaworn, S. Ananta, R. Yimnirun, Mater. Sci. Eng. B 128 (2005) 83.
[20] N. Vittayakorn, G. Rujijanagul, T. Tunkasiri, X. Tan, D.P. Cann, J. Mater. Res. 18 (2003) 2882.
[21] H. Fan, H.-E. Kim, J. Appl. Phys. 91 (2002) 317.